https://doi.org/10.1093/plphys/kiad133 PLANT PHYSIOLOGY 2023: 192: 886–909

Plant Physiology®

Research Article

Autophagy and multivesicular body pathways cooperate to protect sulfur assimilation and chloroplast functions

Yunting Fu,[1] Baofang Fan,[2] Xifeng Li,[1] Hexigeduleng Bao,[1,2] Cheng Zhu[1] and Zhixiang Chen[1,2,*]

1 College of Life Sciences, China Jiliang University, Hangzhou 310018, China
2 Department of Botany and Plant Pathology, Purdue University, West Lafayette, IN 47907-2054, USA

*Author for correspondence: zhixiang@purdue.edu
The author responsible for distribution of materials integral to the findings presented in this article in accordance with the policy described in the Instructions for Authors (https://academic.oup.com/plphys/pages/General-Instructions) is Zhixiang Chen (zhixiang@purdue.edu).

Abstract

Autophagy and multivesicular bodies (MVBs) represent 2 closely related lysosomal/vacuolar degradation pathways. In Arabidopsis (*Arabidopsis thaliana*), autophagy is stress-induced, with deficiency in autophagy causing strong defects in stress responses but limited effects on growth. LYST-INTERACTING PROTEIN 5 (LIP5) is a key regulator of stress-induced MVB biogenesis, and mutation of *LIP5* also strongly compromises stress responses with little effect on growth in Arabidopsis. To determine the functional interactions of these 2 pathways in Arabidopsis, we generated mutations in both the *LIP5* and *AUTOPHAGY-RELATED PROTEIN* (*ATG*) genes. *atg5/lip5* and *atg7/lip5* double mutants displayed strong synergistic phenotypes in fitness characterized by stunted growth, early senescence, reduced survival, and greatly diminished seed production under normal growth conditions. Transcriptome and metabolite analysis revealed that chloroplast sulfate assimilation was specifically downregulated at early seedling stages in the *atg7/lip5* double mutant prior to the onset of visible phenotypes. Overexpression of adenosine 5′-phosphosulfate reductase 1, a key enzyme in sulfate assimilation, substantially improved the growth and fitness of the *atg7/lip5* double mutant. Comparative multi-omic analysis further revealed that the *atg7/lip5* double mutant was strongly compromised in other chloroplast functions including photosynthesis and primary carbon metabolism. Premature senescence and reduced survival of *atg/lip5* double mutants were associated with increased accumulation of reactive oxygen species and overactivation of stress-associated programs. Blocking PHYTOALEXIN DEFICIENT 4 and salicylic acid signaling prevented early senescence and death of the *atg7/lip5* double mutant. Thus, stress-responsive autophagy and MVB pathways play an important cooperative role in protecting essential chloroplast functions including sulfur assimilation under normal growth conditions to suppress salicylic-acid-dependent premature cell-death and promote plant growth and fitness.

Introduction

The growth and survival of all cellular organisms depend on complex networks of trafficking, degradation, and recycling of cellular components. In eukaryotic cells, autophagosomes and multivesicular bodies (MVBs) are well-characterized structures of autophagy and endocytosis, respectively, 2 closely related pathways in the lysosomal/vacuolar degradation system (Fader and Colombo 2009). Autophagy is suppressed under normal growth conditions but is induced upon exposure to stress conditions, such as nutrient starvation (Yin et al. 2016). Induced autophagy is characterized by increased formation of double membrane-bound autophagosomes that transport cytoplasmic components including proteins, organelles, and RNAs for degradation in the lysosomes/vacuoles (Yin et al. 2016). MVBs are single-membrane endosomes in the endocytic pathway for internalization,

Received October 20, 2022. Accepted February 2, 2023. Advance access publication February 28, 2023

sorting, and degradation of plasma membrane proteins (Hanson and Cashikar 2012). MVBs are formed from early endosomes in the endocytic pathway by invagination and budding of the limiting membrane through the action of ESCRT (endosomal sorting complex required for transport) protein complexes (Hanson and Cashikar 2012). The content of MVBs can be degraded through fusion with lysosomes/vacuoles (Hanson and Cashikar 2012).

As 2 closely related lysosomal/vacuolar protein degradation pathways, autophagosomes and MVBs interact extensively (Fader and Colombo 2009; Cui et al. 2018). The maturation process of autophagosomes in some organisms involves fusion with endocytic vesicles, such as MVBs, to form a hybrid organelle called the amphisomes prior to the fusion with lysosomes (Ganesan and Cai 2021). The MVB pathway and autophagy also coordinate in action to promote cell survival upon nutrient starvation in yeast (*Saccharomyces cerevisiae*) cells (Muller et al. 2015). In plant cells, specific components in the MVB pathway are important for the biogenesis, maturation, and trafficking of autophagosomes. Arabidopsis (*Arabidopsis thaliana*) SH3P2 (SH3 domain-containing protein 2), a ubiquitin-binding protein that acts in the transfer of ubiquitinated proteins to the ESCRT machinery (Nagel et al. 2017), also regulates autophagosome expansion and maturation (Zhuang et al. 2013). FREE1 (FYVE domain protein required for endosomal sorting 1), another Arabidopsis protein associated with MVBs through interaction with the ESCRT-I subunit VPS23 (vacuolar protein sorting 23) and ESCRT-III subunit Snf7 (Sucrose non-fermenting protein 7) (Gao et al. 2014), interacts with SH3P2 on autophagosomes (Gao et al. 2015). The mutation of *FREE1* leads to the formation of abnormal MVB-autophagosome hybrid structures, supporting their interaction in plant cells (Gao et al. 2015). During leaf senescence or under nutrient starvation, chloroplast stromal proteins including Rubisco (ribulose-1,5-bisphosphate carboxylase/oxygenase) are transported into the autophagosome-like structures called Rubisco-containing bodies (Izumi et al. 2010; Izumi and Ishida 2011). The ESCRT-III subunit paralogs CHMP1A (charged MVB protein1) and CHMP1B play a direct role in the delivery of Rubisco-containing bodies to the vacuole in Arabidopsis (Spitzer et al. 2015).

Autophagy and MVB pathways also functionally coordinate in plant stress responses (Wang et al. 2020). During plant–pathogen interaction, defense-related molecules including cell surface immune receptors are recruited through MVBs to the plant–pathogen interface (An et al. 2006; Berkey et al. 2017) and this plant–pathogen interaction zone is also a hotspot for autophagosome biogenesis for plant defense (Dagdas et al. 2016; Dagdas et al. 2018). The endocytic MVB and autophagosome pathways also coordinate in the degradation of plasma membrane-localized aquaporin proteins to decrease the water permeability of roots in responses to water-related abiotic stresses under salt, osmotic, and drought conditions (Chaumont and Tyerman 2014). In *Arabidopsis*, salt stress induces endocytosis of aquaporin PIP2;1 (plasma membrane intrinsic protein 2;1) from the plasma membrane to the vacuolar lumen through MVBs in a manner dependent on clathrin, phosphatidylinositol 3-kinase, and phosphatidylinositol 4-kinase (Ueda et al. 2016). Another Arabidopsis aquaporin, PIP2;7, is subjected to degradation by selective autophagy under stress conditions by forming complexes with the multi-stress regulator TSPO (outer membrane tryptophan-rich sensory protein) at the endoplasmic reticulum (ER) and Golgi membranes (Hachez et al. 2014). Through cooperative degradation of newly synthesized aquaporins and plasma membrane-localized PIP aquaporins by selective autophagy and MVB pathway, respectively, plant can rapidly downregulate the water channel proteins at the root cell surface to reduce water loss. Autophagy plays a crucial role in chloroplast protein quality control (QC) and turnover (Fu et al. 2022), whereas MVBs participate in the turnover of specific chloroplast protein precursors to impact plant stress tolerance (Zhang et al. 2022). Autophagy and MVB also cooperate in the regulation of stress responses mediated by plant hormones such as abscisic acid and brassinosteroids (Guillaumot et al. 2009; Yu et al. 2016; Nolan et al. 2017; Zhou et al. 2018; Li et al. 2019).

Unlike autophagy, the endocytic MVB pathway operates at high levels even under normal growth conditions and is essential for plant growth and development (Spitzer et al. 2009; Cui et al. 2016). As a result, Arabidopsis mutants for essential ESCRT components and associated factors such as the SKD1 (SUPPRESSOR OF K^+ TRANSPORT GROWTH DEFECT1) AAA ATPase, which catalyzes the disassembly of the ESCRT-III complex during MVB biogenesis, are lethal (Haas et al. 2007). On the other hand, Arabidopsis knockout mutants for LIP5 (LYST-INTERACTING PROTEIN5), an activator of the SKD1 ATPase, grow and develop normally, indicating that the SKD1 ATPase activity without LIP5 activation is sufficient for MVB biogenesis required for growth and development in Arabidopsis (Wang et al. 2014; Wang et al. 2015). However, the *lip5* mutants are compromised in stress-induced MVB formation, highly susceptible to microbial pathogens and sensitive to abiotic stresses such as salt and heat (Wang et al. 2014; Wang et al. 2015). These results indicate that LIP5 is a key regulator of stress-induced MVB biogenesis in plant responses to both biotic and abiotic stresses. The LIP5 protein is unstable under normal growth conditions but becomes stable upon phosphorylation by stress-responsive MITOGEN-ACTIVATED PROTEIN KINASE3 and 6 (MAPK3 and 6) to promote stress-induced MVB biogenesis (Wang et al. 2014; Wang et al. 2015). MAPK3 and 6 also activate WRKY33 transcription factor through phosphorylation, which, in turn, promotes stress-induced transcription of *AUTOPHAGY-RELATED PROTEIN* (*ATG*) genes (Lai et al. 2011; Mao et al. 2011). Therefore, both stress-induced autophagy and LIP5-regulated MVB biogenesis appear to be regulated coordinately by the MAPK3/6 signaling cascade during plant stress responses.

Despite their strong phenotypes in plant stress responses, Arabidopsis autophagy-deficient *atg* and *lip5* single mutants

are largely normal in plant growth and development. In the present study, we have generated Arabidopsis *atg5/lip5* and *atg7/lip5* double mutants and discovered that they displayed strong synergistic phenotypes in fitness characterized by reduced growth and survival, early senescence, and greatly reduced seed yield even under normal growth conditions. Transcriptome and biochemical analysis indicated that the *atg7/lip5* double mutant was compromised in chloroplast sulfur assimilation at very early stages prior to the appearance of visible phenotypes. Overexpression of a key enzyme in sulfate reduction substantially improved the growth and fitness of the *atg7/lip5* double mutant. Comparative multi-omic analysis also uncovered defects in other important chloroplast functions in the *atg7/lip5* double mutant including photosynthesis and primary carbon metabolism. Premature senescence and reduced survival of the *atg/lip5* doble mutants are associated with increased accumulation of reactive oxygen species (ROS) and overactivation of stress-associated response programs, and are dependent on PHYTOALEXIN DEFICIENT 4 (PAD4)-dependent salicylic acid (SA) production. These findings indicate that basal autophagy and LIP5-regulated MVB pathways play an important cooperative role in protecting important chloroplast functions including sulfate assimilation to suppress defense-related cell death and promote plant growth and fitness.

Results

Synergistic phenotypes of *atg* and *lip5* double mutants in growth and fitness

Under normal conditions, the growth rates and leaf morphology of Arabidopsis autophagy-deficient *atg5* and *atg7* mutants are very similar to those of wild-type (WT) plants during the first 4- to 6-wk post-germination (Yoshimoto et al. 2009; Lai et al. 2011). However, the mutants typically senesce 1 to 2 wk earlier than WT plants (Yoshimoto et al. 2009). Arabidopsis *lip5* mutants have no apparent defects in plant growth and morphology throughout the entire life cycle (Haas et al. 2007; Wang et al. 2014; Wang et al. 2015). The growth and fitness were drastically altered in the *atg7-3/lip5-2* double mutant. Leaf yellowing was not apparent in 4.5- or 5.5-wk-old WT, *atg7* and *lip5* single mutant plants (Fig. 1, A and B) but was very evident in the first 3 leaves of the *atg7/lip5* double mutant (Fig. 1B). In addition, 5- to 6-wk-old *atg7-3/lip5-2* double mutant plants produced more than 10% fewer leaves (Fig. 1B) and were substantially smaller than WT, *atg7-3* and *lip5-2* single mutants (Supplemental Fig. S1A). With increased age, the growth phenotypes of *the atg7-3/lip5-2* mutant plants became more pronounced based on the leaf yellowing, leaf number, and plant size (Fig. 1C; Supplemental Fig. S1A). In addition, about 35% of *atg7-3/lip5-2* plants displayed stunted growth, dehydration, and eventually died in 4- to 6-wk post-germination under normal growth conditions (Supplemental Fig. S1B).

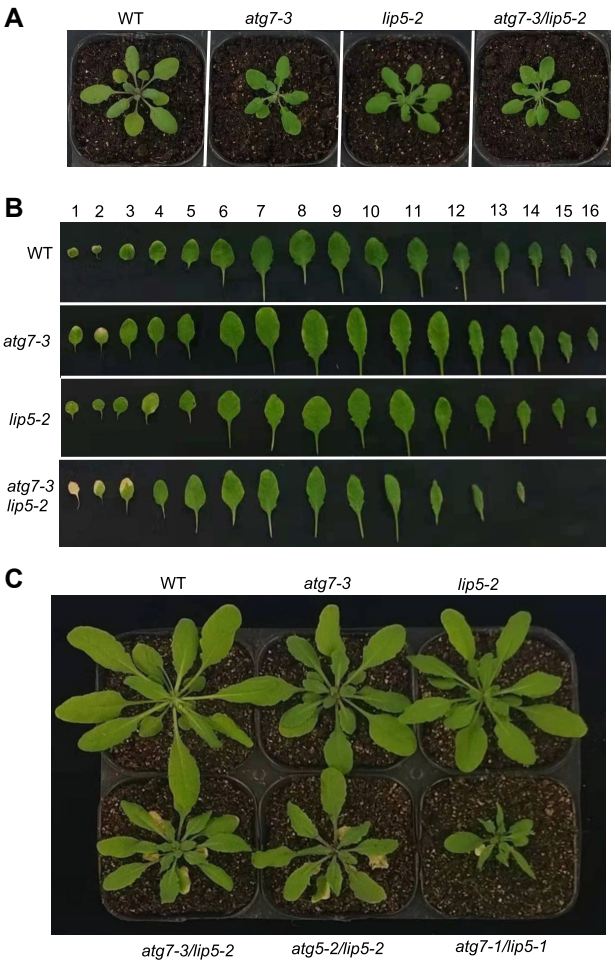

Figure 1. Growth phenotypes of WT, *atg* and *lip5* single and double mutants. Comparison of growth of 4.5-wk-old **(A)**, rosette leaves of 5.5-wk-old **(B)**, and 7-wk-old **(C)** WT, *atg* and *lip5* single and double mutants under normal growth conditions.

For those surviving *atg7-3/lip5-2* double mutant plants, their growth further deteriorated after 5- to 6-wk post-germination, leading to even greater differences in size with WT, *atg7-3* and *lip5-2* mutant plants (Fig. 1C). However, the surviving *atg7-3/lip5-2* double mutant plants were able to flower and produce seeds, even though the size of their siliques and seed yield were greatly reduced when compared with those of WT, *atg7-3* and *lip5-2* single mutants (Fig. 2). We also generated 2 additional double mutants, *atg5-1/lip5-2* and *atg7-1/lip5-1*, *and* observed strong synergistic defects in growth and development similar to those of *atg7-3/lip5-2* (Figs. 1C and 2).

Compromised photosynthesis and chloroplast functions of *atg* and *lip5* mutants under normal and salt-stress conditions

The process of photosynthesis is pivotal to plant growth and development. Given the severely compromised fitness of the *atg/lip5* double mutants and the roles of autophagy and MVB

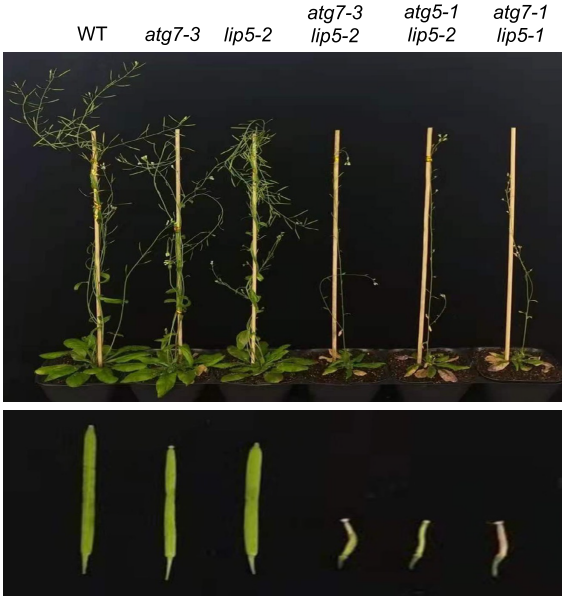

Figure 2. Reproductive phenotypes of WT, *atg* and *lip5* single and double mutants. Comparison of 9-wk-old plants (upper panel) and their representative siliques (lower panel) of WT, *atg* and *lip5* single and double mutants under normal growth conditions.

pathways in chloroplast protein QC (Izumi et al. 2010; Wang and Liu 2013; Michaeli et al. 2014; Spitzer et al. 2015), we compared the *atg7-3/lip5-2* double mutant with their parental single mutants and WT for leaf photosynthetic efficiency. The fifth leaves of 5.5-wk-old WT and mutant plants were determined for the normalized ratio of variable fluorescence over maximum fluorescence (Fv/Fm), which is a measurement for the maximum quantum yield of photosystem II (PSII) (Murchie and Lawson 2013). Even though the first 3 leaves of 5.5-wk-old *atg7-3/lip5-2* double mutant plants already displayed enhanced yellowing relative to WT, *atg7-3* and *lip5-2* single mutants (Fig. 1B), there was little difference in senescence in the fifth leaves among the different genotypes (Figs. 1B and 3A). The Fv/Fm values for the fifth leaves of 5.5-wk-old *atg7-3* and *lip5-2* single mutants were almost the same as those of WT (Fig. 3, A and B). On the other hand, the Fv/Fm for the fifth leaves of 5.5-wk-old *atg7-3/lip5-2* double mutant was about 30% lower than that of WT (Fig. 3, A and B). Thus, unlike the *atg7-3* and *lip5-2* single mutant, the *atg7-3/lip5-2* double mutant had reduced photosynthetic efficiency in leaves prior to the appearance of visible senescence.

Autophagy-deficient mutants and *lip5* mutants are hypersensitive to a variety of abiotic stresses including high salt (Liu et al. 2009; Wang et al. 2015). Germination and growth of Arabidopsis *atg5*, *atg7*, and *lip5* mutants are severely inhibited on ½ Murashige and Skoog (MS) growth medium containing 150 to 160 mM NaCl (Liu et al. 2009; Wang et al. 2015). At 100 mM NaCl, however, the growth of the *atg7-3* and *lip5-2* mutants was little inhibited as indicated by largely normal root and shoot growth (Fig. 3C). On the other hand, the *atg7-3/lip5-2* double mutant displayed extensive bleaching of both cotyledons and emerging rosette leaves when grown at 100 mM NaCl (Fig. 3C). After grown for 18 d at 100 mM NaCl, the chlorophyll content in the *atg7-3* and *lip5-2* single mutants was reduced by about 30% but more than 80% in the *atg7-3/lip5-2* double mutant over those in WT (Fig. 3D). Thus, reduced growth and earlier senescence caused by deficiency of both autophagy and LIP5-regulated MVB biogenesis were associated with reduced accumulation of photosynthetic proteins, and compromised photosynthetic efficiency and other chloroplast functions under both normal and mild salt-stress conditions.

ROS accumulation in *atg* and *lip5* mutants

Chloroplasts and associated biological processes including photosynthesis are both the major producers and targets of cellular ROS (Foyer 2018), which is also one of the earliest responses of plant cells under stress and senescence (Jajic et al. 2015). Given the growth phenotypes, reduced photosynthesis, and enhanced stress- and defense-associated responses, we compared the H_2O_2 levels of the fifth leaves of 5.5-wk-old WT, *atg* and *lip5* single and double mutants using staining with 3,3′-diaminobenzidine (DAB). As indicated earlier, there was little difference in senescence in the fifth leaves of 5.5-wk-old WT and mutant plants (Figs. 1B and 3A). As shown in Fig. 4A, the H_2O_2 levels were normal in the leaves of the *atg7-3* and *lip5-2* single mutants but were substantially elevated in the *atg7-3/lip5-2* double mutant when compared with those in WT. Likewise, the H_2O_2 levels in the leaves of the 2 other *atg/lip5* double mutants were elevated as in the *atg7-3/lip5-2* double mutant (Fig. 4A). Using a more quantitative H_2O_2/peroxidase assay method, we likewise found that the H_2O_2 levels in the fifth leaves of 5.5-wk-old *atg/lip5* double mutants were elevated over those in WT and the *atg7* and *lip5* single mutants (Fig. 4B).

Transcriptomic evidence for enhanced stress response and compromised sulfur assimilation in 4-wk-old *atg7/lip5*

To investigate the molecular basis for the strong growth phenotypes of the *atg/lip5* double mutants, we first compared the transcriptomes of 4-wk-old WT, *atg7-3* and *lip5-2* single and double mutants using RNA-seq analysis. At this age, the *atg7 and lip5* single and double mutants were indistinguishable from those of WT in growth and morphology. Using the cutoff values of $\log_2$(fold change) > 1 or $\log_2$(fold change) < −1 with statistical significance of $P < 0.05$, we identified 713 differentially expressed genes (DEGs) in *atg7-3* versus WT with 198 upregulated and 515 downregulated (Supplemental Fig. S2). A similar number of DEGs (681) were identified in *lip5-2* versus WT with 280 upregulated and 401 downregulated (Supplemental Fig. S2). However, there were 1,040 DEGs in *atg7-3/lip5-2* versus WT with 498 upregulated and 542 downregulated (Supplemental Fig. S2). Thus, the transcriptome of the *atg7-3/lip5-2* double mutant was more altered than those

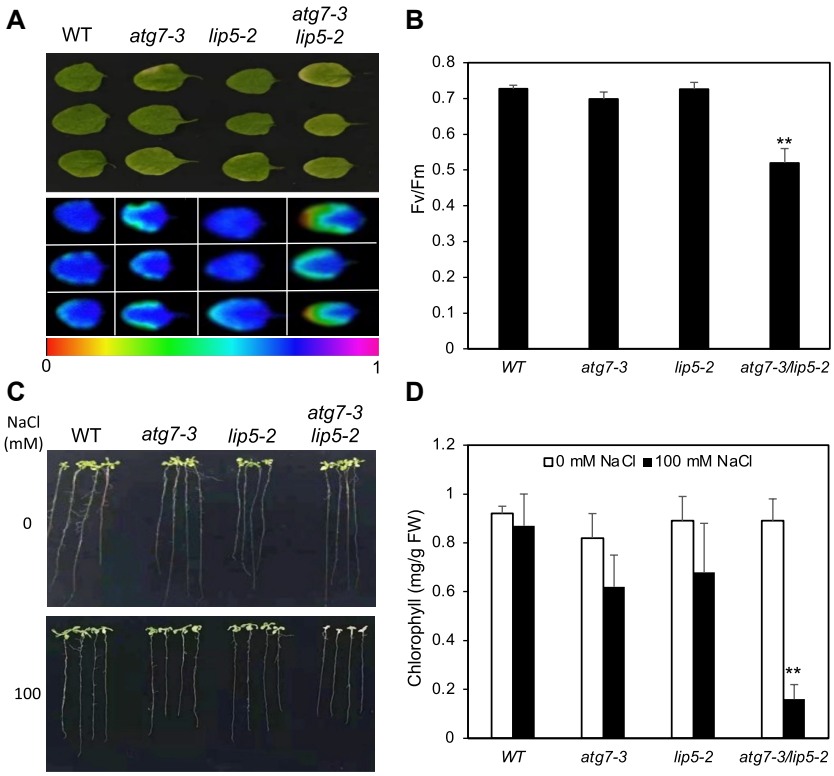

Figure 3. Photosynthetic efficiency and salt tolerance of WT, *atg* and *lip5* single and double mutants. Images **(A)** and values **(B)** of Fv/Fm from the fifth leaves of 5.5-wk-old WT, *atg* and *lip5* single and double mutant plants grown under normal conditions. The scale bar for Fv/Fm value from 0 to 1 is indicated at the bottom. Pictures **(C)** and leaf chlorophyll contents **(D)** of WT, *atg7-3* and *lip5-2* single and double mutant seedlings germinated vertically on ½ MS medium supplemented with 0 or 100 mM NaCl. Error bars for Fv/Fm and chlorophyll content indicate +SE ($n = 5$). **Statistically significant difference at $P < 0.01$ in Fv/Fm or chlorophyll content between WT and a mutant calculated using the Student's *t*-test. These experiments have been repeated twice with similar results. FW, fresh weight.

of the *atg7-3* and *lip5-2* single mutants even at an early age under normal growth conditions. This is consistent with the large numbers of DEGs identified between the *atg7-3* or *lip5-2* single mutant versus the *atg7-3/lip5-2* double mutant (Supplemental Fig. S2). Gene ontology (GO) enrichment analysis indicated that the *atg7-3* and *lip5-2* single and double mutants shared 10 of their top 20 terms of biological processes enriched with identified DEGs (Supplemental Fig. S3A). All these 10 common terms of biological processes were associated with responses to stresses or stress signals including wounding, fungus, jasmonic acid (JA), ethylene, chitin, H_2O_2, and abscisic acid (Supplemental Fig. S3A). These stress and defense-associated processes were also enriched in the DEGs identified between the *atg7-3* or *lip5-2* single mutant versus the *atg7-3/lip5-2* double mutant (Supplemental Fig. S3, B and C). We also performed KEGG (Kyoto encyclopedia of genes and genomes) pathway enrichment analysis and found DEGs in the double mutant to be associated with stress responses and stress-responsive phenylpropanoid, anthocyanin, and other flavonoid biosynthesis and metabolism (Supplemental Fig. S4). Other DEGs are involved in amino acid and fatty acid metabolism (Supplemental Fig. S4), which are known to be regulated by autophagy (Masclaux-Daubresse et al. 2014; McLoughlin et al. 2018; Have et al. 2019; McLoughlin et al. 2020). Importantly, DEGs with the highest statistical significance in the KEGG enrichment also included those involved in sulfur metabolism (Supplemental Fig. S4).

Sulfur is taken up to plant cells by sulfur transporters (SULTR) (Fig. 5A) (Leustek and Saito 1999; Leustek 2002). Members of SULTR subfamily 3 are involved in sulfate transport into plastids (Chen et al. 2019), where sulfur is activated to adenosine 5′-phosphosulfate (APS) by adenosine triphosphate sulfurylase (ATPS) and then reduced by APS reductase (APR) to sulfite, which is further reduced to sulfide by sulfite reductase (Fig. 5A) (Leustek and Saito 1999; Leustek 2002). Sulfide is then incorporated into the amino acid skeleton of *O*-acetylserine to form cysteine. *O*-acetylserine is synthesized from serine and acetyl-Coenzyme A by serine acetyltransferase (SERAT) (Fig. 5A) (Leustek and Saito 1999; Leustek 2002). As shown in Fig. 5B, genes for members of the SULTR sulfur transporters were not substantially altered in expression in the *atg7/lip5* double mutant relative to those in WT. Genes for ATPS1, 2, and 4 were also normal in expression in the *atg7/lip5* double mutant but the expression of *ATPS3* was reduced by almost 70% (Fig. 5B). Notably, transcript levels for all 3 *APR* genes were reduced by 80% to 90% in the *atg7/lip5* double mutant (Fig. 5B). Furthermore, genes involved in response to sulfur starvation and regulation

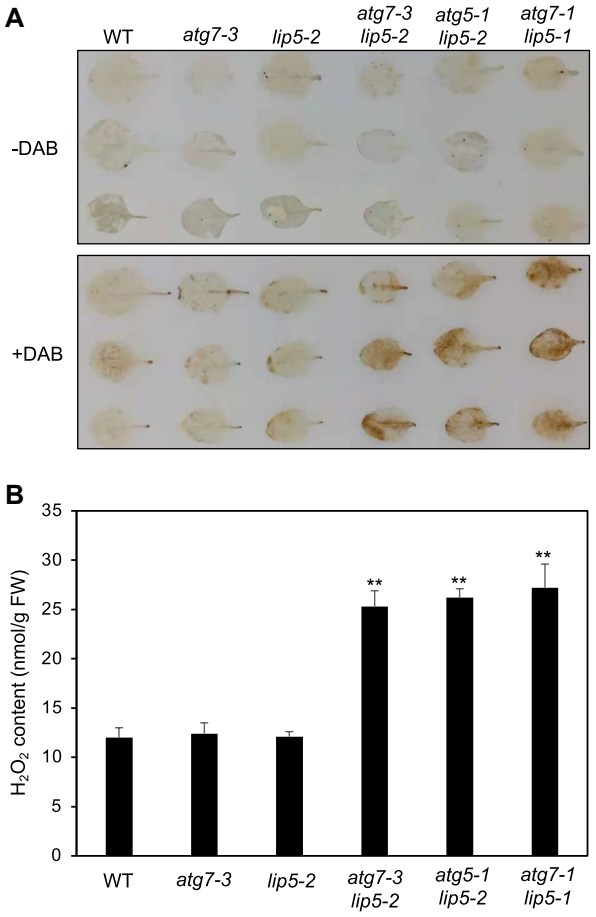

Figure 4. ROS production in WT, *atg* and *lip5* single and double mutants. Production of H_2O_2 in the fifth rosette leaves of 5.5-wk-old WT, *atg* and *lip5* single and double mutant plants were assayed by DAB staining **(A)** or with Amplex Red Reagent **(B)**. Leaves stained in a solution without DAB (-DAB) were included as controls. **Statistically significant difference at $P < 0.01$ between WT and a mutant calculated using the Student's *t*-test. FW, fresh weight.

of sulfur homeostasis were greatly downregulated as well in the *atg7/lip5* double mutants (Fig. 5B). These sulfur responsive genes include all 4 members of the *RESPONSE TO LOW SULFUR* (*LSU*) (Sirko et al. 2014), *MORE SULFUR ACCUMULATION 1* (*MSA1*, also known as *SERINE HYDROXYMEHTYLTRANSFERASE 7* or *SHM7*) (Huang et al. 2016), and 2 members of the *SULFUR DEFICIENCY-INDUCED 1* (*SDI1*) gene family (Howarth et al. 2009) (Fig. 5B). Expression of these sulfur assimilatory and responsive genes were also reduced in the *atg7* and *lip5* single mutants but most of them were more downregulated in the *atg7-3/lip5-2* double mutant (Fig. 5C).

Reduced sulfite and cysteine content in 4-wk-old *atg7/lip5* double mutant

Among the enzymes responsible for sulfate reduction and assimilation, APRs are highly regulated and considered to be a control point for cysteine synthesis (Kopriva et al. 2001; Tsakraklides et al. 2002; Lee et al. 2011). Given the greatly reduced expression of all the 3 *APR* genes, we compared the levels of total sulfur, sulfate, sulfite, and cysteine among 4-wk-old WT, *atg7-3* and *lip5-2* single and double mutants. As shown in Fig. 6A, there was no significant difference in total sulfur levels among WT, *atg7* and *lip5* single mutants. The *atg7/lip5* double mutant had a slight but insignificant increase in total sulfur levels relative to those in WT (Fig. 6A). These results are consistent with the largely normal expression of the SULTR-encoding genes in the mutants (Fig. 5B). Similarly, the levels of sulfate were largely normal in the *atg7* and *lip5* single mutants but significantly elevated in the *atg7/lip5* double mutant (Fig. 6B). The levels of sulfite and cysteine were also normal in the *atg7* and *lip5* single mutants when compared with those in WT (Figs. 6, C and D). In the *atg7/lip5* double mutant, however, both the sulfite and cysteine levels were reduced by more than 30% and 40%, respectively (Fig. 6, C and D). Thus, mutations of both *ATG7* and *LIP5* had a synergistic effect on sulfur reduction and assimilation.

APR1 overexpression improved sulfur assimilation, growth, and fitness of *atg7/lip5*

Cysteine is used for synthesis of proteins, methionine, co-enzymes, and glutathione, which is important for many cellular processes including cellular redox status and stress responses (Davidian and Kopriva 2010; Takahashi et al. 2011; Romero et al. 2014; Kopriva et al. 2019). To determine whether reduced *APR* expression in the *atg7/lip5* double mutant was responsible for its severe phenotypes in growth and fitness, we overexpressed Arabidopsis *APR1* in the double mutant. The *APR1* coding sequence was cloned into a myc-tagged plant transformation vector under the control of the *CaMV 35S* promoter. Because of greatly reduced seed production of the *atg7/lip5* double mutants, which was further exacerbated after Agrobacterium floral dipping, only 3 transgenic lines were obtained after multiple transformation attempts and 1 of them died soon after transfer from the selective growth medium to the soil. Like the *atg7/lip5* double mutant, the 2 transgenic lines (L1 and 2) grew normally during the first 4- to 5-wk post-germination. Unlike the *atg7/lip5* double mutant, however, the transgenic plants did not show early senescence (Fig. 7A). Overexpression of *APR1* also substantially improved but did not completely restore the growth of the *atg7/lip5* double mutant based on both size (Fig. 7A) and biomass (Supplemental Fig. S5). Furthermore, while 30% to 60% *atg7/lip5* double mutant plants died prematurely, all transgenic *atg7/lip5/APR1* plants survived and produced drastically increased numbers of seeds, up to 40% to 60% of those of WT. Reverse-transcription quantitative PCR (RT-qPCR) indicated that transgenic L1 and L2 lines had *APR1* transcript levels about 2- and 8-fold higher than those in WT, respectively. The L2 line also accumulated a higher level of myc-tagged APR1 proteins (Fig. 7B), grew significantly better (Fig. 7A and Supplemental Fig. S5), and produced 50% to 70% more seeds than the L1 line.

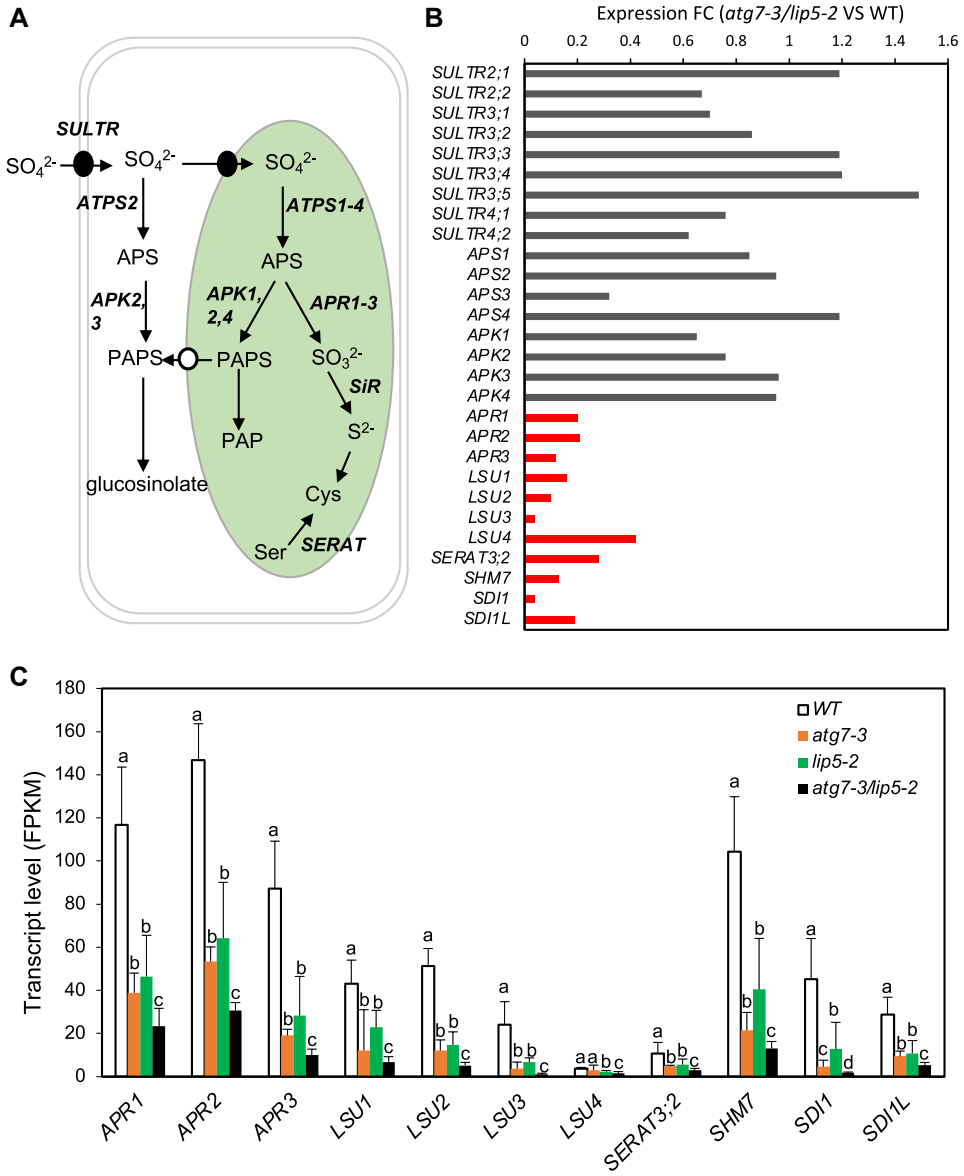

Figure 5. Downregulation of genes involved in sulfur assimilation and low sulfur response in the *atg7-3* and *lip5-2* single and double mutant seedlings. Sulfur transport and assimilation in Arabidopsis **(A)** and the expression fold change (FC) of genes involved in sulfur transport, assimilation, singling, and response in the *atg7-3/lip5-2* double mutant relative over those in WT **(B)**. Transcript levels of those down-regulated sulfur assimilatory and responsive genes in the *atg7-3/lip5-2* double mutant were compared with WT, *atg7-3* and *lip5-2* single mutants **(C)**. Error bars indicate +SE ($n = 3$). According to Duncan's multiple range test ($P < 0.05$), means of transcript levels for each gene do not differ significantly if they are indicated with the same letter.

To determine whether improved growth of the transgenic *atg7/lip5/APR1* plants was associated with enhanced sulfur assimilation, we compared their levels of sulfite and cysteine with those of WT and *atg7/lip5* double mutant. As shown in Fig. 7, C and D, while the levels of sulfite and cysteine were reduced by about 40% in the *atg7-3/lip5-3* double mutant, they were similar to WT levels in the L1 line and were 10% to 20% higher than WT levels in the L2 line (Fig. 7, C and D). These results indicated that reduced capacity of sulfur reduction and assimilation in the *atg7/lip5* double mutant is a critical cause for its early senescence, reduced survival, and compromised fitness. However, the transgenic *atg7/lip5* double mutants overexpressing *APR1* still grew relatively poorly when compared with WT (Fig. 7A and Supplemental Fig. S5), indicating additional defects in the double mutants that impact growth and fitness.

Defects in other chloroplast functions and metabolism in *atg7/lip5*

Upon obtaining transcriptomic evidence for altered stress responses and sulfur assimilation in 4-wk-old *atg7-3* and *lip5-2*

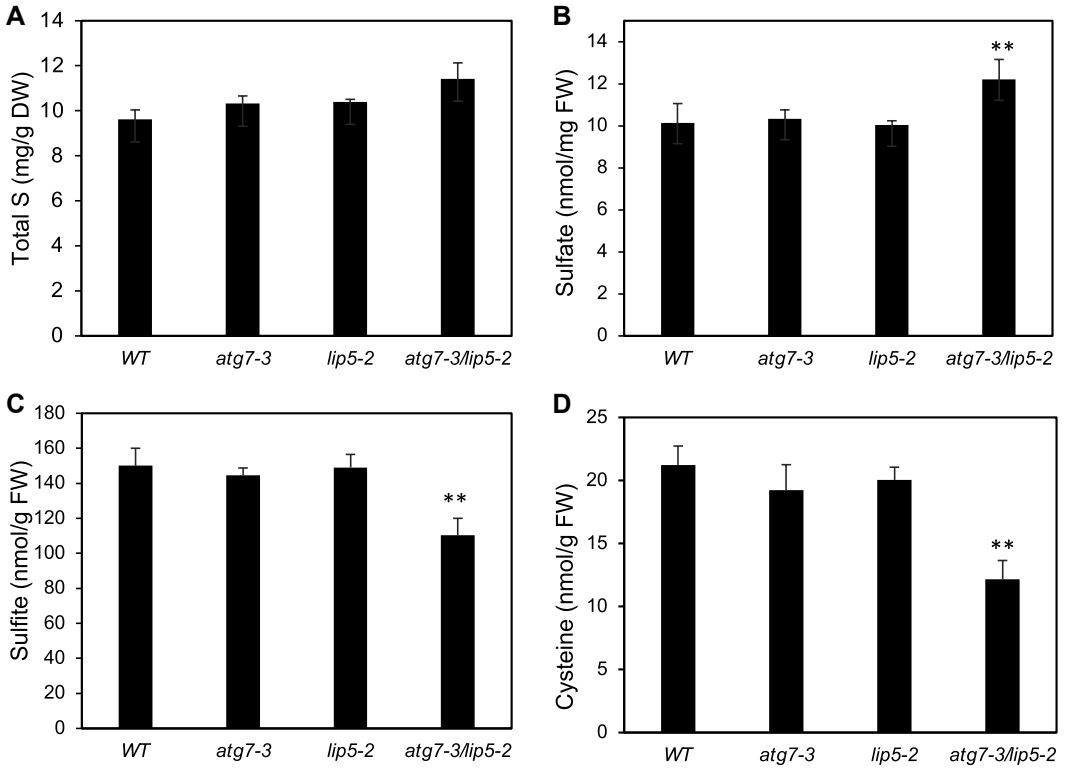

Figure 6. Effects of *atg7-3* and *lip5-2* mutations on sulfur accumulation and assimilation. Aerial parts of 4-wk-old WT, *atg7-3* and *lip5-2* single and double mutant seedlings grown under normal conditions were used to determine the levels of total sulfur **(A)**, sulfate **(B)**, sulfite **(C)**, and cysteine **(D)**. Error bars indicate +SE ($n = 5$). **Statistically significant difference at $P < 0.01$ between WT and a mutant calculated using the Student's *t*-test. DW, dry weight; FW, fresh weight.

mutants, we conducted proteomic profiling of 4-wk-old WT and mutants using Tandem Mass Tag (TMT) mass spectrometry (MS) but only detected a small difference in the proteomes among the genotypes, particularly between the *atg7*/*lip5* double and single mutants. This could be due to a small change in the proteomes relative to the transcriptomes of the mutants at the early growth stage prior to the appearance of visible phenotypes. Proteomic profiling by MS also has a much lower throughput and, consequently, a more limited scope and statistical power than transcriptomic profiling by RNA-seq. Therefore, we performed multi-omics comparison of rosette leaves of 5.5-wk-old WT, *atg7-3* and *lip5-2* single and double mutants. At this age, the *atg7*/*lip5* double mutant plants already started to display minor phenotypes of compromised growth (Fig. 1B). Using quantitative proteomic profiling with 3 biological replicates for each genotype, we identified 29,293 peptides and 4,612 proteins (false discovery rate or FDR < 0.01). Using the ±1.5-fold cutoff value with $P < 0.05$, we identified 334 differentially accumulated proteins (DAPs) in the *atg7* mutant versus WT, with 134 proteins upregulated and 200 downregulated (Supplemental Fig. S6). A similar number of DAPs (336) were identified in the *lip5* mutant versus WT with 133 upregulated and 193 downregulated (Supplemental Fig. S6). However, there were 588 DAPs identified in the *atg7*/*lip5* double mutant versus WT with 292 upregulated and 296 downregulated (Supplemental Fig. S6). From the RNA-seq data of 5.5-wk-old WT and mutant plants, we identified DEGs in the *atg7*, *lip5* single and double mutants versus WT. Using the cutoff values of $\log_2$(fold change) > 1 or $\log_2$(fold change) < −1 with $P < 0.05$, we identified 2,836, 1,144, and 7,058 DEGs of *atg7*, *lip5*, and *lip5*/*atg7* mutants versus WT, respectively (Supplemental Fig. S6). We also compared the metabolite profiles of the rosette leaves of 5.5-wk-old WT, *atg7* and *lip5* single and double mutants using liquid chromatography-MS (LC-MS) with 5 biological replicates from each genotype. We identified 2,312 metabolites, of which 155, 282, and 331 were differentially accumulated metabolites (DAMs) in *atg7*, *lip5*, and *atg7*/*lip5* mutants versus WT, respectively (Supplemental Fig. S6). Based on the numbers of DAPs, DEGs, and DAMs, the proteome, transcriptome, and metabolome of the *atg7*/*lip5* double mutant were most altered, while those of the *lip5* single mutant was least altered from those of WT among the 3 mutants examined. These observations were consistent with the large numbers of DAPs, DEGs, and DAMs identified between the *atg7* or *lip5* single mutant versus the *atg7*/*lip5* double mutant (Supplemental Fig. S6). They were also consistent with the principal component analysis (PCA) of proteomic, transcriptomic, and metabolomic data, which showed that the replicates of the *atg7*/*lip5* double mutant were generally most distant from those of WT

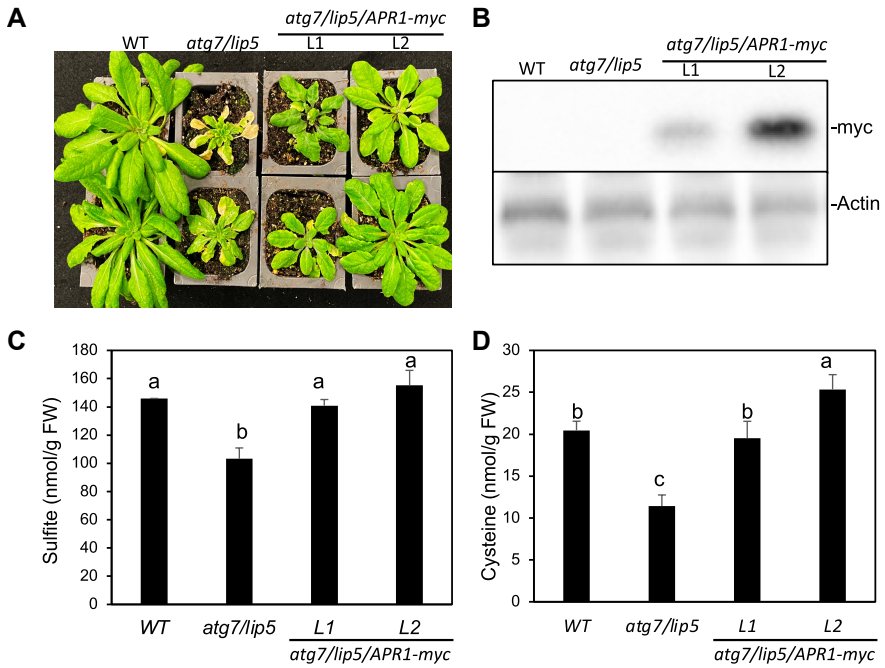

Figure 7. Improvement of growth and sulfur assimilation of the *atg7-3/lip5-2* double mutant by *APR1* overexpression. Plants of WT, *atg7-3/lip5-2*, and the transgenic *APR1* overexpressing lines 1 and 2 (L1 and 2) in the *atg7-3/lip5-2* mutant background were grown under normal growth conditions and were photographed at 7-wk post-germination **(A)**. The levels of myc-tagged APR1 proteins in WT and the *atg7-3/lip5-2* double mutant plants with or without overexpressed *APR1* were detected by protein blotting using anti-myc antibodies **(B)**. Actin proteins detected with an anti-actin antibody were used as protein loading control. Aerial parts of 5.5-wk-old WT, *atg7-3/lip5-2* mutant with or without overexpressed *APR1* grown under normal conditions were used to determine the levels of sulfite **(C)** and cysteine **(D)**. Error bars indicate +SE ($n = 5$). According to Duncan's multiple range test ($P < 0.01$), means do not differ significantly if they are indicated with the same letter. FW, fresh weight.

and clustered closer to those of *atg7* than to those of *lip5* single mutant (Supplemental Fig. S7).

We further analyzed the multi-omics data from WT, *atg7-3* and *lip5-2* single and double mutants to identify important molecular and biochemical processes that were more altered in the *atg7/lip5* double mutant than in the single mutants. As shown in Fig. 8A, 9 of the top 10 categories of biological processes enriched with downregulated DAPs from the *atg7/lip5* double mutant versus WT were associated with photosynthesis and related chloroplast processes including light harvesting, chlorophyll biosynthesis, photosynthetic electron transport, proton transport, starch catabolism, and response to low light intensity. The only other GO term on the top 10 list of biological processes enriched with downregulated DAPs between *atg7/lip5* and WT was anthocyanin biosynthetic process (Fig. 8A). Notably, 4 of the top 10 classes of biological processes enriched with downregulated DEGs from the *atg7/lip5* double mutant versus WT were also associated with photosynthesis and related chloroplast functions (Fig. 8B).

We then performed KEGG enrichment analysis to assign pathways to the DAMs identified from the metabolomic profiling between the *atg7-3/lip5-2* double mutant and WT. As shown in Fig. 8C, among the top 20 identified pathways with significantly enriched DAMs in the *atg7/lip5* double mutant ($P < 0.05$), 10 were directly and at least 4 others were closely associated with amino acid biosynthesis and metabolism. Other significantly altered metabolic processes in the *atg7-3/lip5-2* double mutant included metabolism of glucosinolate, linoleic acid, glutathione, porphyrin, and chlorophyll (Fig. 8C). Importantly, the tricarboxylic acid (TCA) cycle was among the top KEGG pathways that were significantly altered in the *atg7/lip5* double mutant (Fig. 8C). Like photosynthesis in chloroplasts, plant TCA cycle in mitochondria is a vitally important metabolic pathway that regulates cellular redox and energy level and supplies substrates for synthesis of other important components such as amino acids (Zhang and Fernie 2018). Metabolomic profiling indicated that the TCA cycle and amino acid biosynthesis and metabolism were among the top 20 categories of KEGG pathways that were altered in the *atg7-3/lip5-2* double mutant (Fig. 8C). To determine the nature and extent of the changes, we compared the levels of 5 TCA cycle intermediates (citric, fumaric, aconitic, succinic, and isocitric acids) that were detected in the metabolomic profiling among WT, *atg7-3* and *lip5-2* single and double mutants. Mutation of *LIP5* alone had little effect on the levels of the 5 TCA cycle intermediates (Fig. 9). Mutation of *ATG7* alone also had little effect on the levels of citric acid and aconitic acid (Fig. 9). On the other hand, mutation of both *ATG7* and *LIP5* in the *atg7-3/lip5* double mutant reduced the levels of citric acid and aconitic acid by approximately 50% (Fig. 9). The levels of fumaric acid

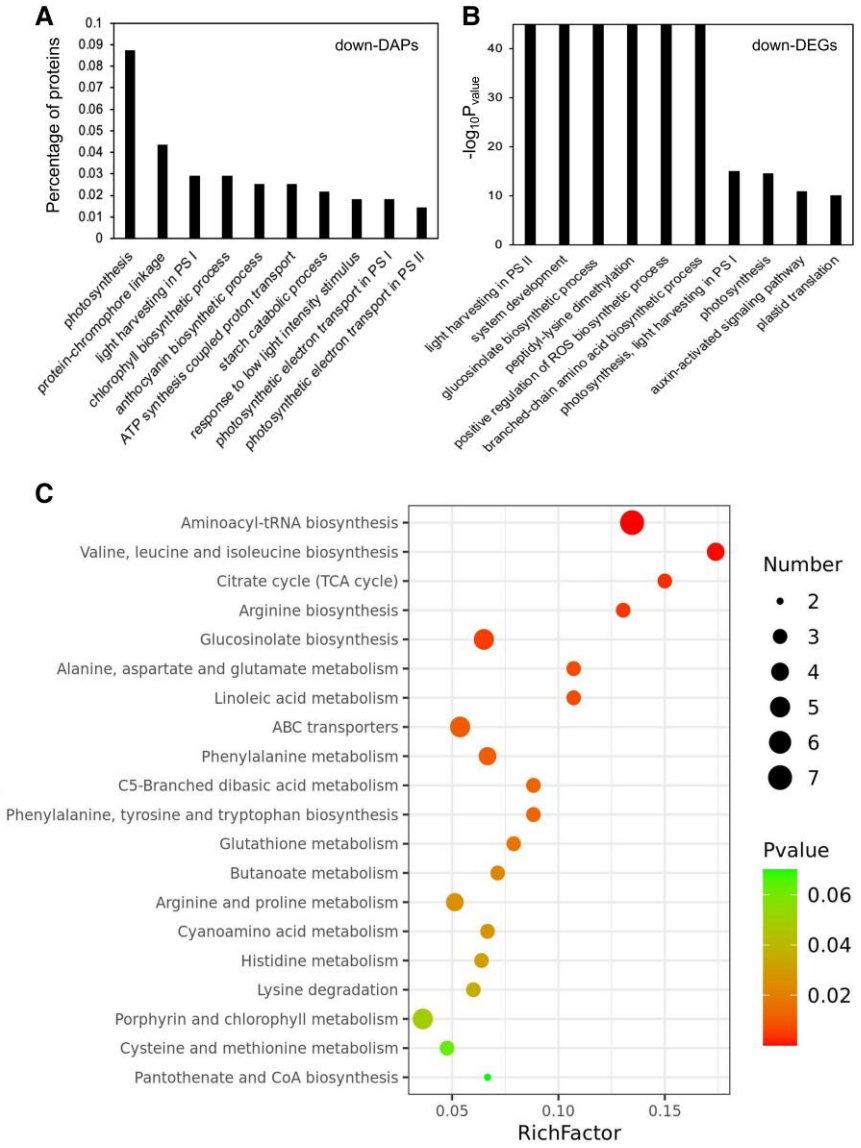

Figure 8. GO and KEGG enrichment analysis of DAPs, DEGs, and DAMs identified between the *atg7-3*/*lip5-2* double mutant and WT at the 5.5-wk-old early adult stage. Top 10 GO categories of biological processes enriched with downregulated DAPs **(A)**, downregulated DEGs **(B)**, and KEGG pathways of DAMs **(C)** identified between the *atg7-3*/*lip5-2* double mutant and WT.

were reduced by 25% in the *lip5-2* mutant but by about 4-fold in the *atg7-3* and *atg7-3*/*lip5-2* mutants (Fig. 9). The levels of succinic acid varied greatly among WT and the mutants; it was slightly reduced in the *lip5-2* single mutant but elevated by more than 10- and 3-fold in the *atg7-3* single and *atg7-3*/*lip5-2* double mutants, respectively (Fig. 9). The levels of isocitric acid were normal in the *lip5-2* single mutant but reduced by about 30% in the *atg7-3* single mutant and 70% in the *atg7-3*/*lip5-2* double mutant (Fig. 9). Thus, among the 6 TCA cycle intermediates detected from metabolomic profiling, 3 (citric, aconitic, and isocitric acids) were preferentially reduced in the *atg7-3*/*lip5-2* double mutant, whereas 1 (fumaric acid) was reduced in both the *atg7-3* single and *atg7-3*/*lip5-2* double mutants (Fig. 9).

Molecular basis for reduced abundance of chloroplast and photosynthetic proteins in the *atg7* and *lip5* mutants

Among the 297 downregulated DAPs in the *atg7-3*/*lip5-2* double mutant, 95 were chloroplast proteins. The average abundance of downregulated chloroplast DAPs was normal in the *lip5-2* single mutant but reduced by 31% and 47% in the *atg7-3* single and *atg7-3*/*lip5-2* double mutants, respectively, over the WT levels (Supplemental Fig. S8). In the *lip5-2* mutant, even though the average protein abundance of the 95 chloroplast DAPs was similar to that in WT, about 50% of the DAPs had significantly increased abundance, whereas the other 50% had reduced abundance relative to those in WT (Supplemental Fig. S9). On the other hand,

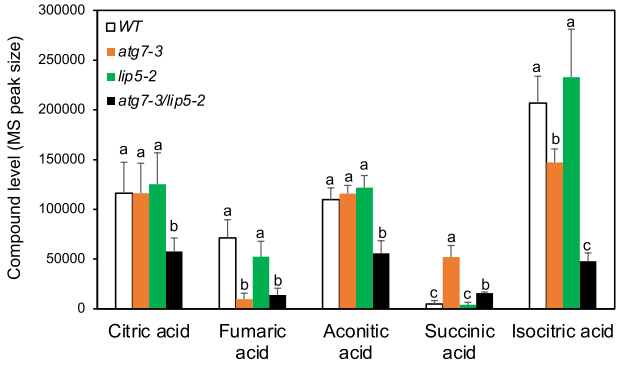

Figure 9. Levels of TCA cycle intermediates in WT, *atg7-3* and *lip5-2* single and double mutants from metabolomic profiling based on the size of the eluted peak for each TCA cycle intermediate from the MS. Error bars indicate +SE ($n = 5$). According to Duncan's multiple range test ($P < 0.01$), means of compound levels for each TCA cycle intermediate do not differ significantly if they are indicated with the same letter.

almost all the 95 chloroplast DAPs had substantially reduced accumulation in the *atg7-3* relative to those in WT and this reduction in abundance was further enhanced for a majority of the 95 DAPs in the *atg7-3/lip5-2* double mutant (Supplemental Fig. S9).

Among the 95 chloroplast DAPs, about 60% were involved in photosynthesis and the remaining DAPs were associated with other biological processes in chloroplasts including sulfate assimilation, protein translation, biosynthetic, and metabolic processes (Supplemental Fig. S9). Among the photosynthetic proteins, 39 are involved in light-dependent reactions including light harvesting, electron transport, NADPH, and ATP synthesis. We compared the levels of the 39 DAPs among WT and the 3 mutants as they constituted the largest group of chloroplast proteins among the 297 identified DAPs. As shown in Fig. 10A, about half of the 39 photosynthetic DAPs were substantially elevated in abundance in the *lip5* mutant over that in WT, while the remaining DAPs were similar to those in WT. On the other hand, the levels of almost all the 39 photosynthetic proteins were reduced by an average of 30% in the *atg7-3* single mutant and about 50% in the *atg7-3/lip5-2* double mutant over those in WT (Fig. 10A). A substantial number of the 39 DAPs were reduced in abundance by more than 60% in the *atg7-3/lip5-2* double mutant over WT levels (Fig. 10A). PAM68 (PHYTOSYNTHESIS AFFECTED MUTANT 68), an Arabidopsis thylakoid protein required for the efficient D1 biogenesis and PSII assembly (Armbruster et al. 2010), was reduced in the *atg7-3/lip5-2* double mutant by more than 70% when compared with that in WT (Fig. 10A).

To determine whether reduced accumulation of the photosynthetic proteins in the *atg7/lip5* double mutant was caused by increased degradation or reduced expression of their corresponding genes, we compared the transcript levels for the nuclear-encoded photosynthetic DAPs among WT and the 3 mutants. As shown in Fig. 10B, transcripts for all the nuclear-encoded photosynthetic DAPs were reduced in the *atg7-3* and *lip5-2* single mutants. The reduction in the transcript levels for the photosynthetic DAPs was generally stronger in the *atg7-3* than in the *lip5-2* single mutant (Fig. 10B). Importantly, the transcript levels for almost all the nuclear-encoded photosynthetic DAPs were substantially lower in the *atg7-3/lip5-2* double mutant than in the *atg7-3* and *lip5-2* single mutants (Fig. 10B). The strong association between the protein and transcript levels for the photosynthetic DAPs suggests that the reduced accumulation of the photosynthetic proteins in the *atg7-3* and *lip5-2* single mutants and, to a greater extent, in the *atg7-3/lip5-2* double mutant has resulted from downregulated expression of the photosynthetic genes.

Upregulation of stress-responsive proteins, transcripts, and metabolites in the *atg7* and *lip5* mutants

Transcriptome profiling of 4-wk-old WT, *atg7-3* and *lip5-2* mutants revealed enhanced upregulation of genes associated with stress signaling and responses in the *atg7-3/lip5-2* double mutant even at early growth stages (Supplemental Fig. S3). Multi-omics analysis of 5.5-wk-old plants also identified enhanced upregulation of stress-responsive proteins, transcripts, and metabolites in the *atg7-3/lip5-2* double mutant relative to the *atg7-3* and *lip5-2* single mutants. First, proteomic profiling identified a substantial number of ER-localized proteins to be upregulated in their abundance in both the *atg7-3* single mutant and, to a greater extent, in the *atg7-3/lip5-2* double mutant (Fig. 11A). By contrast, the levels of these ER proteins were normal or even slightly reduced in the *lip5-2* single mutant relative to those in WT (Fig. 11A). These ER proteins include heat shock proteins (BIP2 and HSP90-7), which are often used as indicators of ER stress. Other upregulated ER proteins included CRT3, PDIL, and AERO2 involved in ER protein QC (Liu and Li 2014), and reticulon-like proteins with possible roles in the regulation of ER homeostasis, including selective ER turnover through autophagy (Zhang et al. 2020).

Proteomic profiling also showed substantial upregulation of 2 cell wall-modifying enzymes involved in cell separation during development (ADPG1 and 2) in the *atg7-3/lip5-2* double mutant, but not in the *atg7-3* and *lip5-2* single mutants (Fig. 11B). PBS3, a key SA biosynthetic enzyme (Torrens-Spence et al. 2019), and SAG12, a cysteine protease and senescence protein marker involved in nitrogen allocation (James et al. 2018), were normal in the *lip5-2* single mutant, but were elevated in both the *atg7-3* single mutant and, to a much greater extent, in the *atg7-3/lip5-2* double mutant (Fig. 11B). Direct comparison of transcript levels for the 3 DEGs involved in pipecolic acid biosynthesis (FMO1, ALD1, and SARD4) (Mishina and Zeier 2006; Ding et al. 2016; Jiang et al. 2021) indicated that their expression was not altered in the *lip5-2* single mutant, but again was elevated in

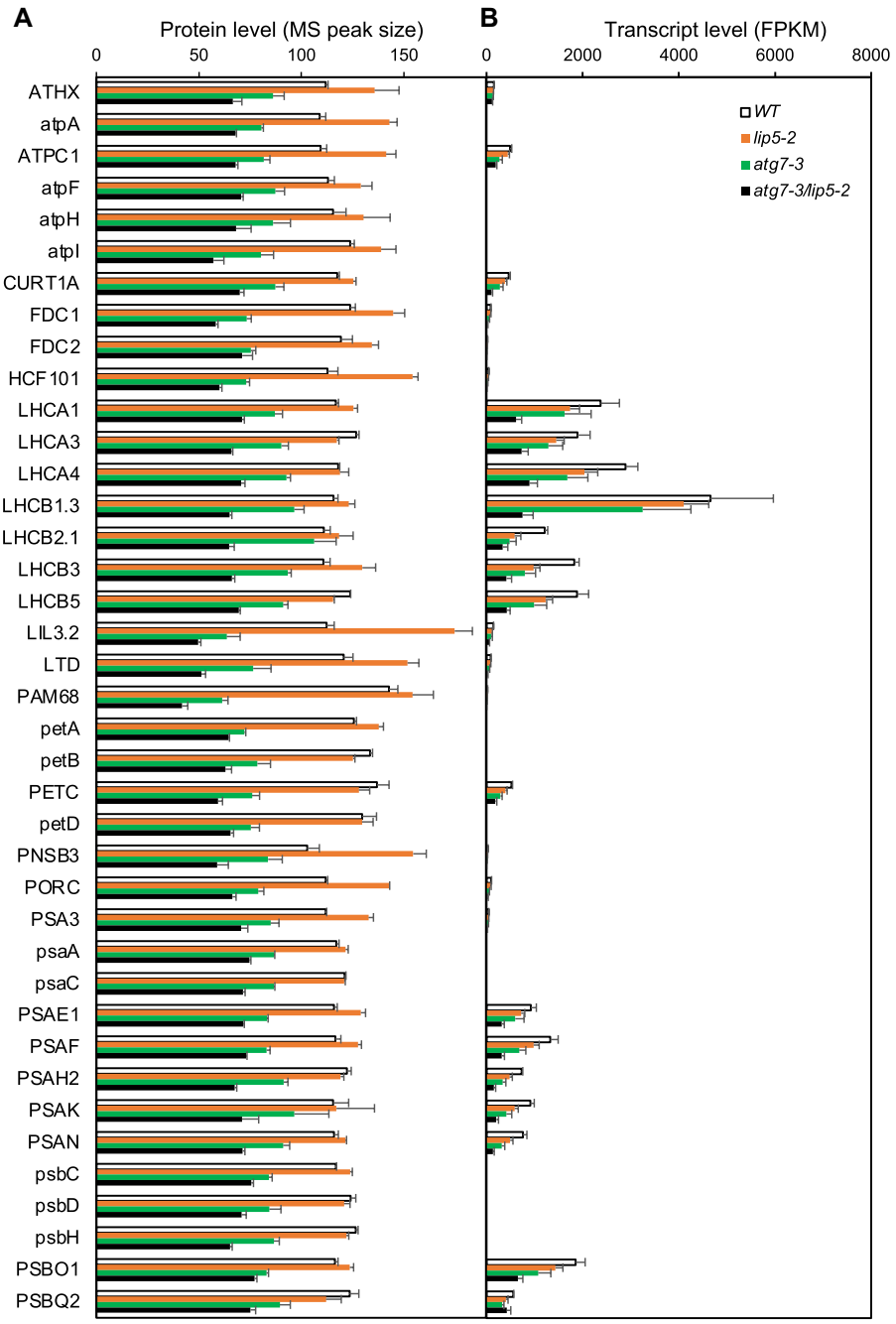

Figure 10. Downregulation of photosynthetic proteins in the *atg7-3* and *lip5* single and double mutants. Protein levels of photosynthetic DAPs based on MS peak size (left) and the transcript levels of their corresponding genes based on fragments per kilobase of exon per million mapped fragment (FPKM) (right) in WT, *atg7-3* and *lip5-2* single and double mutants. Chloroplast-encoded photosynthetic proteins written in low case didn't have data of transcript levels from the transcriptomic profiling. Error bars indicated +SE ($n = 3$).

the *atg7-3* single mutant and, to a greater extent, in the *atg7-3*/*lip5-2* double mutant (Fig. 11C).

Consistent with the upregulation of proteins and transcripts associated with stress- and senescence-related signaling and responses, the levels of SA and pipecolic acid detected from metabolomic profiling were elevated in the *atg7-3* but not in the *lip5-2* single mutant (Fig. 11D). The increased accumulation of SA and pipecolic acid in the *atg7-3* single mutant was substantially enhanced in the *atg7-3*/*lip5-2* double mutant (Fig. 11D). Metabolomic profiling also indicated that the levels of another signaling molecule, JA, were substantially elevated in the *atg7-3*/*lip5-2* double mutant, but not in the *atg7-3* or *lip5-2* single mutant (Fig. 11D).

Mutations of both *ATG7* and *LIP5* reduced the content of cysteine at early seedling stages (Fig. 6D). To assess the effect of deficiency of autophagy and LIP5-regulated MVB

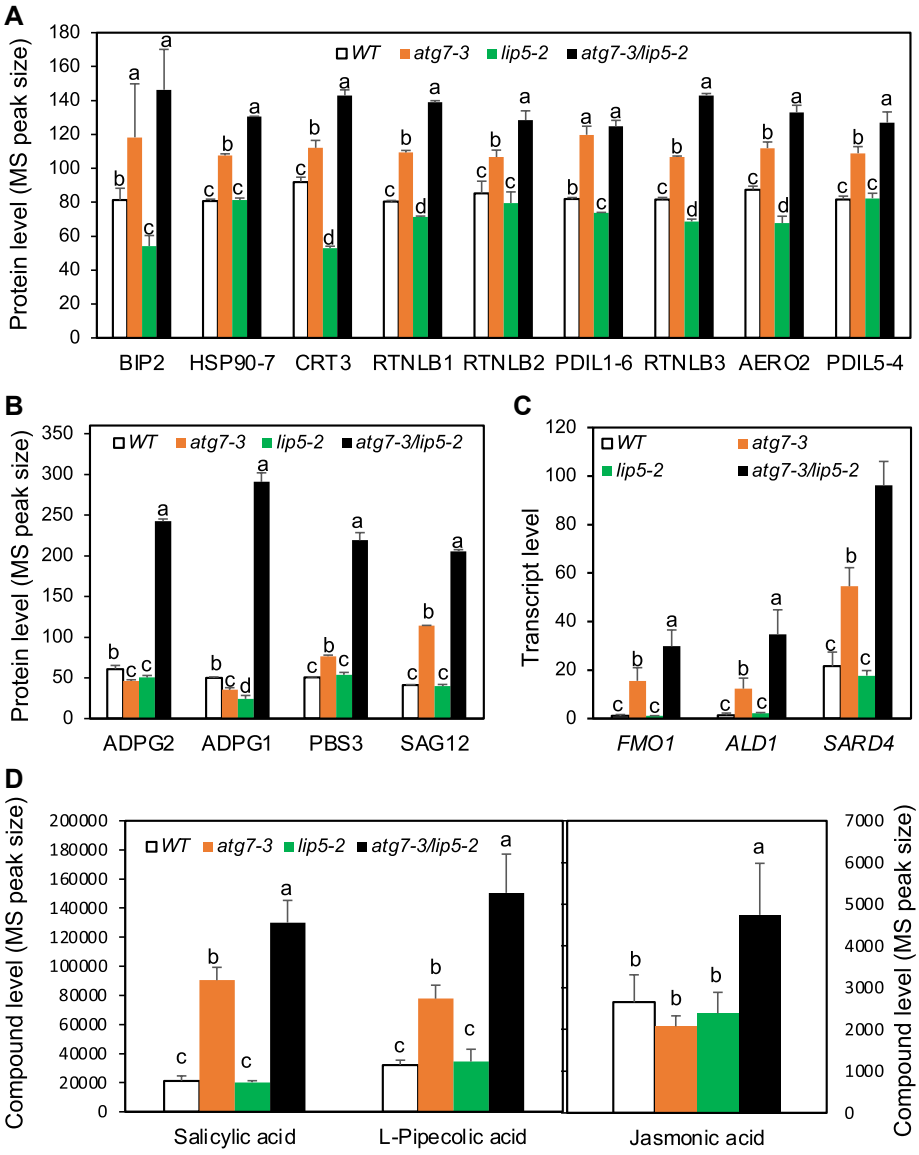

Figure 11. Upregulation of proteins, transcripts, and metabolites associated with stress signaling and responses. Protein levels of ER stress-associated DAPs **(A)**, DAPs associated with senescence and SA biosynthesis **(B)**, transcript levels of DEGs involved in pipecolic acid biosynthesis **(C)**, and the levels of SA, pipecolic acid, and JA **(D)**. Error bars indicated +SE calculated from 3 replicates ($n = 3$) for protein and transcript levels and 5 replicates ($n = 5$) for metabolite (compound) levels. According to Duncan's multiple range test ($P < 0.01$), means do not differ significantly if they are indicated with the same letter for each protein, gene, or metabolite.

biogenesis on biosynthesis and metabolism of other amino acids, we compared the levels of 15 amino acids that were detected from metabolomic profiling among WT, *atg7* and *lip5* single and double mutants. Generally, mutation of *LIP5* alone had little effect on the levels of the 15 amino acids (Fig. 12). Even though autophagy deficiency can negatively affect the levels of amino acids due to reduced protein degradation, the levels of the 15 amino acids were not substantially reduced in the *atg7-3* mutant when compared with those in WT (Fig. 12). In fact, the levels of some amino acids including aspartic acid, glutamic acid, isoleucine, lysine, methionine, and tyrosine were substantially elevated under the normal growth conditions in the autophagy-deficient mutant (Fig. 12), as reported previously (Masclaux-Daubresse et al. 2014; McLoughlin et al. 2018; Have et al. 2019; McLoughlin et al. 2020). Interestingly, among the 15 detected standard amino acids, the levels of proline were normal in the *atg7-3* and *lip5-2* single mutants but were 16 times higher than those in WT in the *atg7-3/lip5-2* double mutant (Fig. 12). Increased accumulation of proline is a well-recognized response to various environmental stresses and plays protective roles as an osmoprotectant, stabilizer of cellular structures, and scavenger of ROS (Hayat et al. 2012). The levels of tryptophan were also increased by 2-fold in the *atg7-3/lip5-2* double mutant but were unaltered in the *atg7-3* and *lip5-2* single mutants (Fig. 12). Tryptophan is often the least

abundant amino acid in the cell and the precursor for a variety of important molecules including auxin, camalexin, glucosinolate, melatonin, and serotonin. Isoleucine levels were elevated in the *atg7-3* mutant by about 50% but more than doubled in the *atg7-3/lip5-2* double mutant (Fig. 12).

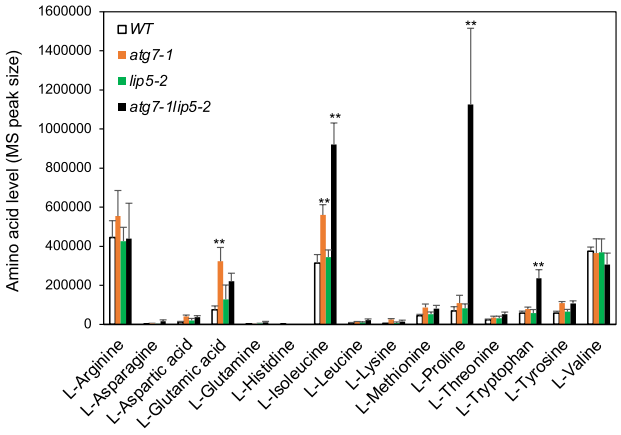

Figure 12. Levels of amino acids in WT, *atg7-3* and *lip5-2* single and double mutants from metabolomic profiling based on the size of the eluted peak for each amino acid from the MS. Error bars indicated +SE ($n = 5$). **Statistically significant difference at $P < 0.01$ between WT and a mutant for each amino acid calculated using the Student's *t*-test.

Roles of SA signaling and its relationship with sulfur assimilation in the synergistic growth phenotypes of *atg7/lip5*

SA is a signal molecule with an important role in plant defense, growth, and growth-defense crosstalk (Zhong et al. 2021). PAD4 is a lipase-like protein with an important role in SA signaling and in both basal and resistance gene-mediated plant defense responses (Rietz et al. 2011; Cui et al. 2017). To determine the role of SA- and PAD4-mediated defense signaling in severely compromised growth and fitness of the *atg/lip5* double mutants, we crossed SA-deficient *sid2* and *pad4* mutants with the *atg7-3/lip5-2* double mutant and generated the *atg7/lip5/sid2* and *atg7/lip5/pad4* triple mutants, respectively. Like the *atg7/lip5* double mutant, the *atg7/lip5/sid2* and *atg7/lip5/pad4* triple mutants grew normally during the first 4- to 5-wk post-germination. However, the triple mutants did not show early senescence (Fig. 13A). The growth of the triple mutants was also substantially improved but was not completely restored to the levels of WT based on both size (Fig. 13A) and biomass (Fig. 13A and Supplemental Fig. S10). Furthermore, all the *atg7/lip5/sid2* and *atg7/lip5/pad4* triple mutant plants survived and generated about 60% of seeds produced by WT. The improved growth and fitness of the *atg7/lip5/sid2* and *atg7/lip5/pad4* triple mutants over the *atg7/lip5* double mutant were strikingly similar to those of the transgenic *atg7/lip5* double mutants overexpressing *APR1* (Fig. 7A and Supplemental Fig. S5).

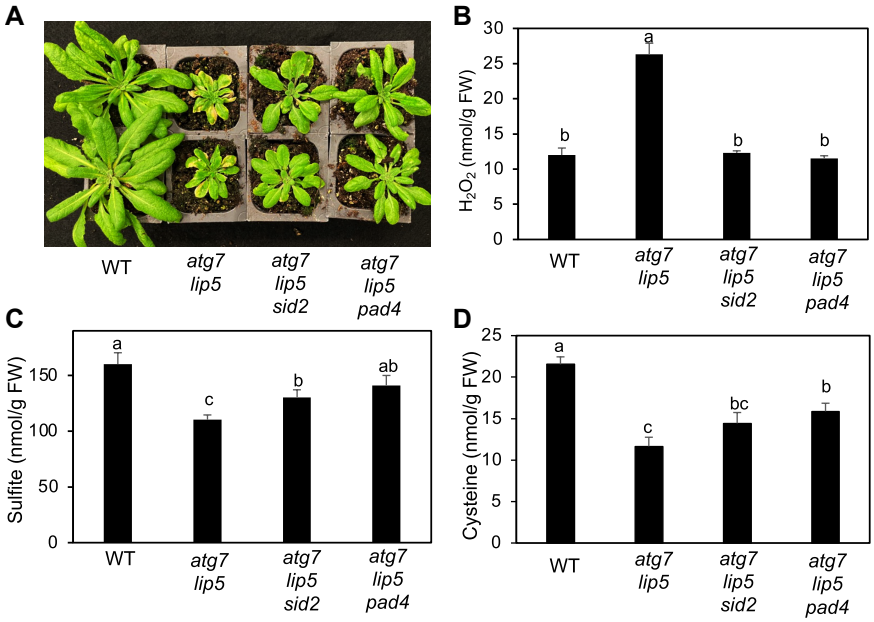

Figure 13. Roles of PAD4 and SA signaling in compromised growth and sulfur assimilation in the *atg7-3/lip5-2* double mutant. Plants of WT, *atg7-3/lip5-2* double mutant, *atg7-3/lip5-2/sid2* and *atg7-3/lip5-2/pad4* triple mutants were grown under normal growth conditions and were photographed at 7-wk post-germination **(A)**. Production of H_2O_2 in the fifth rosette leaves of 5.5-wk-old WT and mutant plants were assayed with Amplex Red Reagent **(B)**. Aerial parts of the plants grown under normal conditions were used to determine the levels of sulfite **(C)** and cysteine **(D)**. Error bars indicate +SE ($n = 5$). According to Duncan's multiple range test ($P < 0.01$), means do not differ significantly if they are indicated with the same letter. FW, fresh weight.

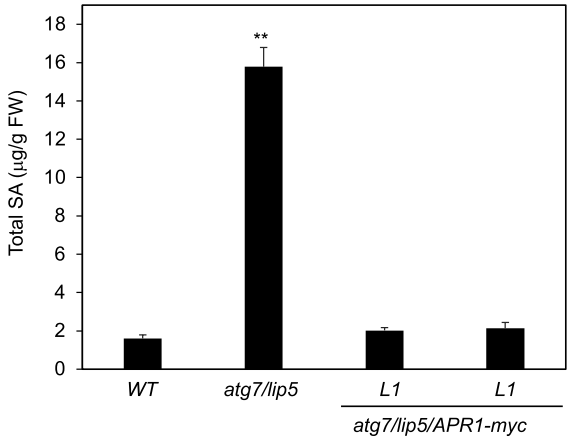

Figure 14. Effects of *APR1* overexpression on SA accumulation in the *atg7-3/lip5-2* double mutant. Plants of WT, *atg7-3/lip5-2*, and the transgenic *APR1* overexpressing lines 1 and 2 (L1 and 2) in the *atg7-3/lip5-2* mutant background were grown under normal growth conditions. Aerial parts of 7-wk-old WT, *atg7-3/lip5-2* mutant with or without overexpressed *APR1* grown under normal conditions were used to determine the levels of total SA. Error bars indicate +SE ($n = 6$). **Statistically significant difference at $P < 0.01$ between WT and a mutant calculated using the Student's *t*-test. FW, fresh weight.

To determine whether improved growth of the *atg7/lip5/sid2* and *atg7/lip5/pad4* triple mutants was associated with reduced ROS accumulation and enhanced sulfur assimilation, we compared their levels of H_2O_2, sulfite, and cysteine with those in WT and *atg7/lip5* double mutant. Unlike in the *atg7/lip5* double mutant, the H_2O_2 levels in the 5th leaves of the 5.5-wk-old *atg7/lip5/sid2* and *atg7/lip5/pad4* triple mutants were similar to those in WT (Fig. 13B). In addition, as shown in Fig. 13, C and D, while the levels of sulfite and cysteine were significantly elevated in the *atg7/lip5/sid2* and *atg7/lip5/pad4* triple mutants over those of the *atg7/lip5* double mutant, they were still substantially lower than those in WT. This was particularly true with the levels of cysteine, which were about 30% lower in the 2 triple mutants than in WT (Fig. 13D). Thus, PAD4 and SA signaling may act independently or downstream of sulfur assimilation in the regulation of the growth and fitness in the *atg7/lip5* double mutant. To distinguish between these possibilities, we analyzed the effects of APR1 overexpression on the SA accumulation in the *atg7/lip5* double mutants. As found from the metabolome profiling, the SA levels were elevated by 10-fold in the *atg7/lip5* double mutant over those in WT (Fig. 14). Overexpression of *APR1* almost completely restored the SA levels in the *atg7/lip5* double mutants to the levels in WT (Fig. 14). Thus, defective sulfur assimilation played a critical role in enhanced SA accumulation in the *atg7/lip5* double mutant.

Discussion

Despite their strongly compromised disease resistance and abiotic stress tolerance, knockout mutants for Arabidopsis ATG proteins and LIP5 are largely normal in growth, development, and seed production. Several groups have reported multi-omics analysis of autophagy-deficient mutants in Arabidopsis and maize and discovered extensive alteration in transcriptomes, proteomes, and metabolomes in autophagy-deficient mutants under normal growth conditions, despite very limited phenotypes in growth and morphology (Masclaux-Daubresse et al. 2014; McLoughlin et al. 2018; Have et al. 2019; McLoughlin et al. 2020). This strong cellular adaptability of autophagy-deficient mutants is apparently no longer sufficient to maintain robust plant growth and fitness in the *atg/lip5* double mutants with the additional deficiency of LIP5-regulated MVB pathway (Figs. 1 and 2). Unlike the *atg* and *lip5* single mutants, the *atg/lip5* double mutants were severely compromised in growth and fitness characterized by reduced growth, early senescence, reduced survival, and greatly diminished seed yield under normal growth conditions (Figs. 1 and 2). Therefore, autophagy and LIP5-activated MVB pathway play a vital role not only in plant survival under stress conditions but also in plant growth and fitness under normal conditions. Apparently, these stress-responsive protection mechanisms also operate at basal levels under normal growth conditions with a previously underappreciated important role in plant growth and development.

Autophagy and LIP5-activated MVB pathway participate in plant defense and stress responses by targeting degradation of damaged, harmful, and unwanted proteins and cellular constituents, which are often elevated under biotic and abiotic stress conditions. Autophagy, for example, targets the degradation of protein aggregates that are generated under stress conditions such as high temperature (Zhou et al. 2013; Zhou et al. 2014). MVB biogenesis may promote endocytic degradation of plasma membrane-localized transporter proteins to reduce salt uptake under high salinity (Wang et al. 2015) or target turnover of specific chloroplast proteins to impact heat tolerance (Zhang et al. 2022). Under normal growth conditions, cells also generate damaged, harmful, or unwanted cellular proteins. In the ER, about 30% of all proteins produced are misfolded under homeostatic conditions (Fink 1999), which are mostly degraded by ER-associated degradation (READ) in the proteasome. Accumulation of misfolded proteins in the ER can lead to ER stress and the activation of unfolded protein response and autophagy (Zeng et al. 2019; Bao and Bassham 2020). In chloroplasts, the process of photosynthesis leads to the production of damaged proteins under normal growth conditions, which are removed by both intraplastidic proteases and extraplastidic pathways including autophagy (Izumi and Nakamura 2018; Fu et al. 2022). Therefore, cellular homeostasis is also constantly challenged by intrinsic cellular processes under normal growth conditions. While a number of protein QC pathways including ERAD, intraplastidic proteases, and autophagy are known to play roles in cellular response to intrinsic physiological stress and aging, their impacts on plant productivity have not been fully appreciated due to the

largely normal macroscopic traits in size, biomass, and seed yield of their loss-of-function mutants. The synergistic phenotypes of the atg/lip5 double mutants over their parental single mutants in growth and fitness indicate a complex functional relationship among these related protein QC pathways that has masked their critical roles in plant growth, development, and fitness.

Based on the comprehensive comparative analysis of WT, *atg*, *lip5* single and double mutants, we have revealed that compromised chloroplast functions including sulfur reduction and assimilation play a major role in the strong synergistic phenotypes of the *atg*/*lip5* double mutants (Fig. 15). Even at 4-wk-old seedling stages prior to the appearance of visible phenotypes, defects in sulfur assimilation were already evident based on the greatly reduced expression of all 3 members of the APR gene family and other genes in sulfur response and homeostasis (Fig. 5). As a result, both sulfite and cysteine, the products of sulfate reduction and assimilation, were substantially reduced in the *atg7*/*lip5* double mutant at seedling stages (Fig. 6, C and D). Amino acid cysteine is utilized not only in protein synthesis but also as a precursor for the cellular redox buffer glutathione (Droux 2004). Sulfur metabolism also produces sulfated compounds such as glucosinolates and sulfated peptides, as well as other by-products such as 3′-phosphoadenosine 5′-phosphate (PAP) with roles in chloroplast-to-nucleus retrograde signaling (Fig. 5A) (Chan et al. 2019). The metabolism of cysteine can also result in the production of hydrogen sulfide (H_2S), a signaling molecule that mitigates stress and regulates important plant processes such as photosynthesis, stomatal movement, and autophagy (Chan et al. 2019; Aroca et al. 2021; Gotor et al. 2021). Overexpression of *APR1*, a key enzyme in sulfate reduction, restored the levels of both sulfite and cysteine, suppressed both early senescence and premature death, and greatly improved seed yield of the *atg7*/*lip5* double mutant (Fig. 7). These findings indicate that compromised sulfate reduction is a critical factor responsible for the synergistic phenotypes of the *atg*/*lip5* double mutants in both growth and reproduction (Fig. 7).

As a metabolic process important for the cellular redox state, sulfur assimilation affects cellular ROS levels (Andres-Barrao et al. 2021), which were substantially elevated in the *atg*/*lip5* double mutants (Fig. 4). ROS accumulation causes oxidative damage and eventually leads to cell death (Van Breusegem and Dat 2006; Yoshimoto et al. 2009; Mittler et al. 2022), which were also observed at increased levels in the *atg*/*lip5* double mutants relative to their parental single mutants and WT plants. ROS also act as key players in the signaling network of plant defense and stress responses (Mittler et al. 2022). Like sulfur assimilation, induction of defense and stress-related genes was already apparent at seedling stages prior to the appearance of visible senescence (Supplemental Fig. S3). The overactivated defense/stress-related responses in the *atg*/*lip5* double mutants were associated with increased levels of stress-related proline and signaling molecules including SA, pipecolic acid, and JA (Figs. 11 and 12). Deficiency in PAD4 and SA signaling suppressed the development of early senescence and premature death of the *atg7*/*lip5* double mutant with limited effect on the cysteine levels (Fig. 13). On the other hand, overexpression of *APR1* not only restored sulfur assimilation but also suppressed both the accumulation of SA and development of early senescence and premature cell death in the *atg7*/*lip5* double mutant (Figs. 7 and 14). These results support a proposed model that defective sulfur assimilation from very early seedling stages in the *atg7*/*lip5* double mutants leads to compromised cellular redox homeostasis and increased ROS accumulation, which activated the PAD4- and SA-dependent stress response. Since mutations of PAD4 and SID2 in the *atg7*/*lip5* double mutant also reduced ROS accumulation, PAD4/SA signaling and ROS can mutually promote each other to produce an amplification loop to promote senescence and cell death (Fig. 15).

There were also enhanced defects in other important chloroplast functions and associated metabolic pathways in the *atg7*/*lip5* double mutants. In particular, the *atg7*/*lip5* double mutant, but not its parental single mutants, displayed reduced photosynthetic rates in the leaves with no visible senescence symptoms (Fig. 3). The reduced photosynthetic efficiency of the double mutant was associated with downregulated accumulation of photosynthetic proteins involved in light-harvesting, photosystem reaction center proteins, electron transport, ATP synthesis, and starch synthesis (Fig. 10). Photosynthesis provides plants with energy and carbohydrates and as such can impact other primary metabolic pathways including the TCA cycle, which is an important part of respiration for generation of energy, reducing agent NADH and precursors for biosynthesis of amino acids (Athanasiou et al. 2010; Allakhverdiev 2020). The levels of the TCA cycle intermediates were substantially downregulated in the *atg7*/*lip5* double mutants relative to those in WT and the *atg7* and *lip5* single mutants (Fig. 9). Strong defects in both photosynthesis and respiration likely also play a key role in the strong phenotypes of the *atg*/*lip5* double mutants in growth and fitness (Fig. 15).

Besides the identification of defective chloroplast functions and sulfur assimilation as the primary reasons for the strong synergistic phenotypes of the *atg*/*lip5* double mutants in growth and fitness, our comprehensive investigation has provided insight into the signaling and responses of plant cells to perturbed chloroplast protein homeostasis. Multi-omics analysis revealed that there was a strong association between the protein and transcript levels for downregulated photosynthetic proteins (Fig. 10). Reduced APR protein levels in sulfate reduction were also associated with greatly reduced transcript levels for all 3 members of the APR gene family (Fig. 5 and Supplemental Fig. S9), which led to reduced capacity in sulfate reduction and assimilation in the *atg*/*lip5* double mutants (Fig. 6). Therefore, reduced abundance of most chloroplast proteins in the *atg* and *lip5* mutants resulted from their reduced expression (Fig. 15). Apparently, defects in chloroplast protein homeostasis as a

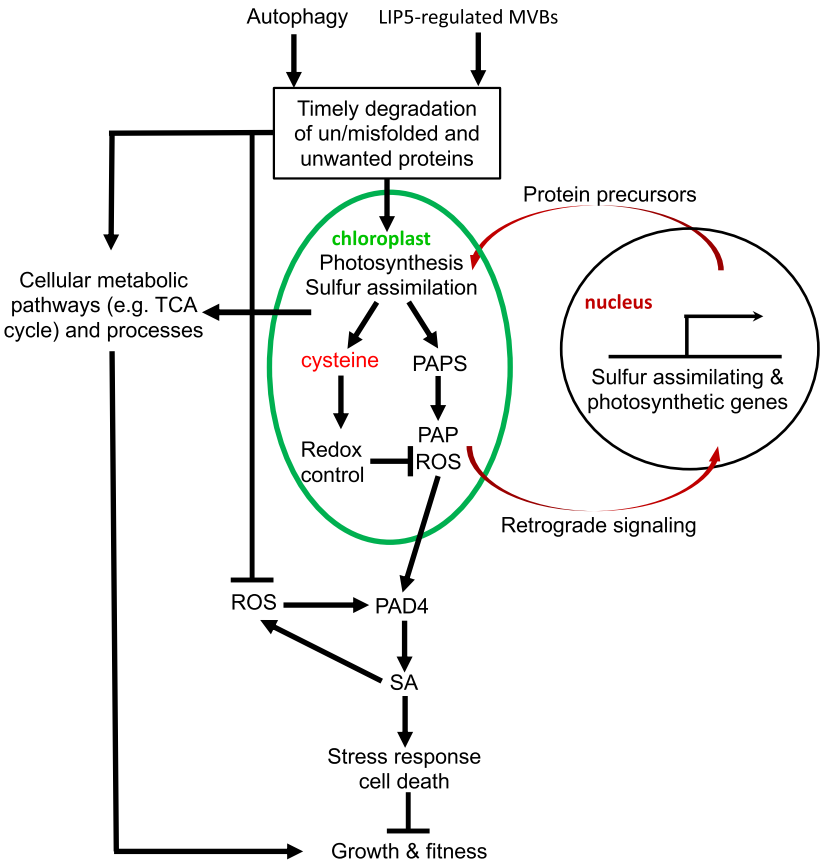

Figure 15. A model for the cooperative regulation of plant growth and fitness by autophagy and LIP5-regulated MVB pathways. Autophagy and LIP5-activated MVB biogenesis protect chloroplast functions including sulfur assimilation through the degradation of un/misfolded and unwanted proteins that are generated from the operation of chloroplasts under normal growth conditions. Chloroplast sulfur assimilation leads to the production of cysteine, which is used for the synthesis of a variety of metabolites for important cellular processes including redox and ROS control. Autophagy, LIP5-regulated MVBs, and protected chloroplast functions also promote other metabolic pathways and cellular processes to promote plant growth and fitness. Defects in sulfate reduction could lead to increased levels of PAPS, the precursor of PAP, which together with ROS could function as chloroplast retrograde signals to regulate expression of nuclear-encoded chloroplast sulfur-assimilating and photosynthetic genes. Compromised protein QC in the cytosol in the autophagy and *lip5* mutants could also lead to increased ROS from other sources, which together with chloroplast ROS could lead to PAD4-dependent SA stress signaling. SA can further elevate ROS levels to produce an amplification loop to promote cell death and negatively affect plant growth and fitness.

result of deficiency in both autophagy and LIP5-regulated MVB biogenesis can trigger retrograde signaling to influence transcription of nuclear-encoded chloroplast genes including those involved in sulfur assimilation and photosynthesis.

Chloroplast retrograde signaling is vital for chloroplast biogenesis and operation (Chan et al. 2016; Zhao et al. 2019). Operational chloroplast retrograde signaling is for adjustments to chloroplast and cellular homeostasis in response to perturbation in chloroplast functions due to both external and internal stimuli (Chan et al. 2016). Among the well-established operational chloroplast retrograde signals are ROS and PAP (Chan et al. 2016), both of which could be impacted in the *atg/lip5* double mutants (Fig. 15). Perturbation in photosynthesis, as observed in the *atg/lip5* double mutants, could result in the formation of H_2O_2 and superoxide ($O_2^{\cdot-}$) at photosystem I and singlet oxygen ($^1O_2$) at PSII (Rizhsky et al. 2003; Triantaphylides and Havaux 2009; Ramel et al. 2012). PAP is formed from a by-product of sulfur assimilation, 3′-phosphoadenosine 5′-phosphosulfate (PAPS), which, in turn, is generated from APS catalyzed by APS kinase (APK) (Fig. 5A) (Phua et al. 2018). APS is also the substrate for APRs in the primary sulfur metabolism pathway (Fig. 5A) and reduced APR protein levels could conceivably increase the conversion of APS to PAPS and PAP through the secondary sulfur metabolism pathway (Figs. 5 and 15). Interestingly, both ROS and PAP as chloroplast operational retrograde signals also participate in such physiological processes as cell death mediated by JA and SA (Chan et al. 2016), which were elevated and played a critical role in the synergistic growth phenotypes of the *atg/lip5* double mutants (Figs. 11 and 13). Photosynthetic ROS can increase the production of JA and β-carotene-derived $O_2^{\cdot-}$ products such as β-cyclocitral, which, in turn, can enhance SA synthesis (Ramel et al. 2013; Lv et al. 2015; Duan et al. 2019). JA and PAP

can also promote each other's production, possibly through a positive feedback regulatory mechanism (Rodriguez et al. 2010). JA and its precursor 12-oxo-phytodieonic acid can also induce PAP for retrograde signaling (Kopriva 2013). Sulfur starvation, which can be invoked by high PAP levels (Lee et al. 2012), induced JA biosynthetic genes (Hirai et al. 2003; Maruyama-Nakashita et al. 2003; Nikiforova et al. 2003). Mutation of *SAL1* (*SALT TOLERANCE 1*) (Quintero et al. 1996), which encodes an enzyme that degrades PAP, increased the levels of both PAP and JA (Rodriguez et al. 2010). Thus, defects of chloroplast function including photosynthesis and sulfur assimilation in the *atg/lip5* double mutants can generate ROS and PAP that can potentially influence the expression of nuclear-encoded chloroplast genes and trigger SA- and JA-dependent stress responses to activate cell death. Further investigation will be necessary to test these specific chloroplast retrograde signals for their roles in the strong phenotypes of growth and fitness resulted from the deficiency of both autophagy and LIP5-activated MVB biogenesis in the *atg/lip5* double mutants.

Materials and methods

Plant materials and growth conditions

The Arabidopsis (*A. thaliana*) mutants and WT plants used in the study are all in the *Col-0* background. The *atg5-2*, *atg7-1*, *atg7-3*, *lip5-1*, and *lip5-2* mutants have been previously described (Lai et al. 2011; Wang et al. 2014). The *pad4* (Salk_206548) and *sid2* (Salk_042603) T-DNA insertion mutants were obtained from the Arabidopsis Resource Center at the Ohio State University and confirmed using PCR genotyping with gene-specific primers flanking the insertion sites (*pad4*: 5′-CCTCTGCTCGGAAACCAATC-3′ and 5′-CTGATGCATCGCAACGATCT-3′; *sid2*: 5′-CCGCCACTGAAAGGCTAATC-3′ and 5′-CTGGCCCACAAAACACAAAA-3′). The *atg5/lip5*, *atg7/lip5*, *atg7-3/lip5-2/pad4*, and *atg7-3/lip5-2/sid2* double and triple were produced by genetic crossing of appropriate mutants and identified in the F2 generation using PCR genotyping with gene-specific primers. Primers used for genotyping *atg5*, *atg7*, and *lip5* mutants were the same as previously described (Lai et al. 2011; Wang et al. 2014). Arabidopsis were grown in growth chambers or rooms at 24 °C, 120 μE $m^{-2}s^{-1}$ light on a photoperiod of 12-h light and 12-h dark.

RNA isolation and RNA-seq

Total RNA was extracted from rosette leaves of 4- and 5.5-wk-old WT, *atg7-3* and *lip5-2* single and double mutants (3 replicates for each genotype) using the TRIzol reagent according to the manufacturer's protocol. RNA purity and quantification were evaluated using the NanoDrop 2000 spectrophotometer (Thermo Scientific, USA). RNA integrity was assessed using the Agilent 2100 Bioanalyzer (Agilent Technologies, Santa Clara, CA, USA). The libraries were constructed using TruSeq Stranded mRNA LT Sample Prep Kit (Illumina, San Diego, CA, USA) according to the manufacturer's instructions. The libraries were sequenced on an Illumina HiSeq X Ten platform and 150 bp paired-end reads were generated. Raw data (raw reads) of fastq format were first processed using Trimmomatic (Bolger et al. 2014) and the low-quality reads were removed to obtain the clean reads. The clean reads were mapped to the Arabidopsis reference genome using HISAT2 (Kim et al. 2019). FPKM (fragments per kilobase of exon per million mapped fragment) of each gene was calculated using Cufflinks (Ghosh and Chan 2016), and the read counts of each gene were obtained by HTSeq-count (Anders et al. 2015; Putri et al. 2022). Differential expression analysis was performed using the DESeq2 R package (Love et al. 2014). $P < 0.05$ and fold change > 2 or fold change < 0.5 were set as the threshold for significantly differential expression. The RNA-seq data for both 4- and 5.5-wk-old WT and mutants have been deposited in the NCBI database with the BioProject numbers PRJNA757606 and PRJNA756793, respectively.

Proteomic profiling by TMT-MS

Proteins were extracted from rosette leaves (3 replicates for each genotype), quantified by BCA (bicinchoninic acid) method, and examined for quality by sodium dodecyl sulfate polyacrylamide gel electrophoresis. For digestion, proteins (100 μg) were first dissolved in 120 μl reducing buffer containing 5 mM dithiothreitol, 8 m urea, and 100 mM triethylammonium bicarbonate (TEAB), pH 8.0 and incubated at 60 °C for 1 h. Iodoacetamide was added to the solution with the final concentration of 50 mM in the dark for 40 min at room temperature. The solutions were centrifuged on the filters at 13,500 × *g* for 20 min at 4 °C and the flow-through solution was discarded from the collection tubes. The filters were washed twice with 100 μl TEAB (300 mM) and then transferred into new collection tubes. After adding 100 μl TEAB (300 mM), 3 μl sequencing-grade trypsin (1 μg μl^{-1}) was added to each tube and the solutions were incubated for digestion at 37 °C for 12 h. The solutions of digested peptides were collected by centrifugation and lyophilized. For TMT labeling, the lyophilized samples were resuspended in 100 μl TEAB (200 mM) and 40 μl of each sample was transferred into a new tube for TMT labeling according to the manufacturer's protocol. Briefly, 88 μl acetonitrile were added to a TMT reagent vial at room temperature. The TMT label reagent (41 μl) was then added to each peptide mixture and incubated at room temperature for 1 h. The reaction was terminated by adding 8 μl of 5% (w/v) hydroxylamine. The labeling peptide solutions were lyophilized and stored at −80 °C.

Peptide fractionation was performed on an 1100 HPLC System (Agilent) using an Agilent Zorbax Extend reverse-phase (RP) column (5μm, 150 mm × 2.1 mm). Mobile phases A (2% v/v acetonitrile) and B (98% v/v acetonitrile) were used for the RP gradient. The separated peptides were lyophilized for MS performed by a Triple TOF 5600 mass spectrometer equipped with a Nanospray III source (SCIEX, USA). Data

were acquired with a 2.4 kV ion spray voltage, 35 psi curtain gas, 5 psi nebulizer gas, and an interface heater temperature of 150 °C. The MS/MS data were analyzed for protein identification and quantification using ProteinPilot software (v.5.0). The local FDR was estimated with the integrated PSPEP tool in the ProteinPilot Software (Shilov et al. 2007) to be 1.0% after searching against a decoy concatenated UniProt Arabidopsis protein database. Only proteins identified at global FDR $\leq$ 1% and unique peptides $\geq$ 1 were considered for protein lists and for further downstream analysis. DAPs were identified and quantified with at least 1 significant peptide and the *P*-values of the protein quantitation should be less than 0.05 and fold change $\geq$ 1.5. The MS proteomics data have been deposited to the ProteomeXchange Consortium (http://proteomecentral.proteomexchange.org) via the iProX partner repository with the dataset identifier PXD028132.

Metabolomic profiling by LC-MS

For metabolite extraction, leaf samples (80 mg, 5 replicates for each genotype) were transferred to 1.5 ml Eppendorf tubes. L-2-chlorophenylalanine (0.3 mg ml^{-1}) in methanol as internal standard and 1 ml mixture of methanol and water (4:1, vol/vol) were added to each sample. Samples were extracted by ultrasonic for 30 min in an ice-water bath and stored at −20 °C for overnight. The extract was centrifuged at 4 °C (15,800 × *g*) for 10 min. The supernatant was transferred to LC vials and stored at −80 °C until LC-MS analysis. QC samples were prepared by mixing an aliquot of all samples to be a pooled sample. ACQUITY UPLC HSS T3 column system coupled with VION IMS QTOF Mass spectrometer (Waters Corporation, Milford, USA) was used to analyze the metabolic profiles in both ESI positive and negative ion modes. An ACQUITY UPLC HSS T3 column (100 mm × 2.1 mm, 1.8 μm) was employed in both positive and negative modes. Water and acetonitrile/methanol (2:3, v/v), both containing 0.1% (v/v) formic acid were used as mobile phases A and B, respectively.

Data acquisition was performed in full scan mode (*m*/*z* ranges from 50 to 1000) combined with MS^E mode, including 2 independent scans with different collision energies alternatively acquired during the run. The QCs were injected at regular intervals throughout the analytical run to provide a set of data from which repeatability can be assessed. The original LC-MS data were processed by software Progenesis QIV2.3 (Nonlinear, Dynamics, Newcastle, UK) for baseline filtering, peak identification, integral, retention time correction, peak alignment, and normalization. Compound identification wase based on precise mass-to-charge ratio (*M*/*z*), secondary fragments, and isotopic distribution. The extracted data were then further processed by removing any peaks with a missing value (ion intensity = 0) in more than 50% of ingroups, by replacing the zero value by half of the minimum value, and by screening according to the qualitative results of the compound. Compounds with resulting scores below 36 (out of 60) points were also deemed to be inaccurate and removed. A data matrix was combined from the positive and negative ion data and was imported in R to carry out PCA to observe the overall distribution among the samples and the stability of the whole analysis process. Orthogonal Partial Least-Squares-Discriminant Analysis (OPLS-DA) and Partial Least-Squares-Discriminant Analysis were utilized to distinguish the metabolites that differ between groups. To prevent overfitting, 7-fold cross-validation and 200 Response Permutation Testing were used to evaluate the quality of the model. Variable Importance of Projection (VIP) values obtained from the OPLS-DA model were used to rank the overall contribution of each variable to group discrimination. A two-tailed Student's *t*-test was further used to verify whether the metabolites of difference between groups were significant. Differential metabolites were selected with VIP values greater than 1.0 and *P*-values less than 0.05.

Other bioinformatic analysis

GO enrichment and KEGG pathway enrichment analyses were performed using R with the CLUSTERPROFILER and PATHVIEW packages (Yu et al. 2012; Luo and Brouwer 2013).

Analysis of total Sulfur, sulfate, sulfite, and cysteine contents

For measurement of total sulfur content, fresh Arabidopsis leaves were harvested, washed with deionized water, and dried at 7 °C. Dried samples (10 mg) were weighted and analyzed for total sulfur content by a Carbon-Hydrogen-Nitrogen-Sulfur (CHNS) Elemental Analyzer (Model Thermo Finnigan FlashEA 1112, Thermo Fisher Scientific, San Jose, CA) by following the manufacturer's instructions. Determination of sulfate content was performed as previously described (Liang et al. 2010). Briefly, fresh leaves were homogenized in 5 to 10 volumes of 0.01 M HCl (fresh weight basis). After centrifugation at 15,000 × *g* for 10 min at 4 °C, supernatants were collected and used for the determination of sulfate content using the turbidimetric method with K_2SO_4 as a standard (Tabatabai and Bremner 1970). The sulfite and cysteine contents in fresh leaves were analyzed by HPLC after derivation with monobromobimane as previously described (Volkel and Grieshaber 1992; Tsakraklides et al. 2002).

Overexpression of *APR1* in the *atg7*/*lip5* double mutant

The coding sequence for the Arabidopsis *APR1* gene was PCR-amplified using gene-specific primers (5′-agcctcgagATGGCAATGTCTGTAAATGTTTCT-3′ and 5′-agcttaattaaTCGGACAAGATTCAAGAACGAA-3′) and cloned between the *CaMV 35S* promoter and a 4× myc epitope sequence in a pGFC1008-derived binary vector as previously described (Wang et al. 2019). The APR1 overexpression construct was transformed into the *atg7*/*lip5* double mutant plants using the floral dipping method. Transgenic plants were identified

by hygromycin resistance and analyzed for expression of the *APR1* gene by both RT-qPCR and protein blotting.

RT-qPCR

Total RNA isolation, DNase treatment, cDNA synthesis, and RT-qPCR using gene-specific primers were performed with *ACTIN2* as an internal control as described previously (Kim et al. 2008).

Protein blotting

Preparation of total leaf proteins, protein quantification, electrophoretic fractionation, blotting, and immunoblot analysis with an anti-myc monoclonal antibody (Sigma, St Louis, MO, USA) were performed as previously described (Li et al. 2021). Actin proteins probed with an anti-actin monoclonal antibody (Sigma) were used as a loading control.

Analysis of chlorophyll fluorescence

Measurement of maximal quantum yield of PSII (Fv/Fm), through chlorophyll fluorescence imaging, was performed with a pulse amplitude modulated fluorometer (IMAG-MAXI; Heinz Walz) as previously described (Huang et al. 2010).

Assays of H_2O_2 content

The histochemical staining of H_2O_2 was performed as previously described (Thordal-Christensen et al. 1997) with minor modifications. Briefly, leaf discs were vacuum infiltrated with 0 or 1 mg ml^{-1} DAB in 0.2 M HCl and incubated at 25 °C in dark for 4 to 5 h on a shaker at 80 to 100 rpm. Leaf discs were then rinsed in bleaching solution (ethanol:acetic acid:glycerol = 3:1:1; v/v) for 15 min at 90 to 95 °C before photographing. H_2O_2 content was also measured using an Amplex Red Hydrogen Peroxide/Peroxidase Assay Kit (Thermo Fisher Scientific). For sample preparation, 0.5 g leaf tissues were ground in liquid nitrogen and thoroughly mixed with 10 volumes of 50 mM Na_3PO_4 (pH 7.4). After centrifugation at 13,500 × *g* for 20 min at 4 °C, the supernatants were used for the H_2O_2 assay following the manufacturer's instructions.

Assays of salt sensitivity and chlorophyll content

The seeds were directly germinated on 1/2 MS medium supplemented with 0 or 100 mM NaCl. Eighteen days after germination, the seedlings were photographed. For measurement of leaf chlorophyll content, roots were removed from the seedlings and chlorophyll was extracted from the remaining parts of the seedlings using 95% (v/v) ethanol and the chlorophyll content of the filtered solution was determined spectrophotometrically as previously described (Porra et al. 1989).

SA analysis

Total SA levels in the leaf samples were determined with a biosensor strain *Acinetobacter* species, *ADPWH_lux*, and calculated based on the SA standard curve constructed using the *sid2* mutant leaf extract as described previously (Huang et al. 2010).

Accession numbers

Arabidopsis Genome Initiative numbers for the genes discussed in this article are as follows: ATG5 (AT5g17290), ATG7 (AT5g45900), LIP5 (AT4g26750), APR1 (At4g04610), APR2 (At1g62180), APR3 (AT4g21990), SID2 (At1g74710), PAD4 (At3g52430), and COPT6 (At2g26975), ACTIN2 (AT3g18780). RNA-seq data for 4- and 5.5-wk-old WT and mutants have been deposited in the NCBI database with the BioProject numbers of PRJNA757606 and PRJNA756793, respectively. MS proteomics data have been deposited to the ProteomeXchange Consortium (http://proteomecentral.proteomexchange.org) via the iProX partner repository with the dataset identifier PXD028132.

Acknowledgments

We thank the Arabidopsis Resource Center at the Ohio State University for providing the mutants used in the study.

Author contributions

C.Z. and Z.C. conceived the original research plans and supervised the experiments; Y.F. and B.F. performed most of the experiments; X.L. and H.B. performed some of the experiments; Y.F., C.Z., and Z.C. analyzed the data and wrote the article with contributions of all the authors.

Supplemental data

The following materials are available in the online version of this article.

Supplemental Figure S1. Effect of *atg7-3* and *lip5-2* mutations on plant growth and survival.

Supplemental Figure S2. Numbers of up and downregulated differentially expressed genes (DEGs) among 4-wk-old wild-type (WT) and *atg7-3* and *lip5-2* single and double mutant seedlings.

Supplemental Figure S3. Gene ontology (GO) enrichment analysis of differentially expressed genes (DEGs) identified between the *atg7* and *lip5* single or double mutants and wild-type (WT) plants at the 4-wk-old seedling stage.

Supplemental Figure S4. KEGG (Kyoto encyclopedia of genes and genomes) pathway enrichment analysis of differentially expressed genes (DEGs) identified between the *atg7-3*/*lip5-2* double mutant and wild-type (WT) at the 4-wk-old early adult stage.

Supplemental Figure S5. Biomass of aerial parts of 7-wk-old wild-type (WT) plants, *atg7-3*/*lip5-2*, and its transgenic lines 1 (L1) and 2 (L2) overexpressing *APR1*.

Supplemental Figure S6. Number of up and downregulated differentially accumulated proteins (DAPs), differentially expressed genes (DEGs), and differentially accumulated metabolites (DAMs) among 5.5-wk-old wild-type (WT)

seedlings and *atg7-3* and *lip5-2* single and double mutant seedlings.

Supplemental Figure S7. Principal component analysis (PCA).

Supplemental Figure S8. Mean protein abundances of the 95 chloroplast DAPs in 5.5-wk-old wild-type (WT) plants, *atg7-3* and *lip5-2* single mutants, and *atg7-3/lip5-2* double mutants.

Supplemental Figure S9. Fold change (FC) in protein abundance of the 95 chloroplast DAPs in 5.5-wk-old *lip5-2* and *atg7-3* single and double mutants over those in wild-type (WT) plants.

Supplemental Figure S10. Biomass of aerial parts of 7-wk-old wild-type (WT) plants, *atg7-3/lip5-2* double mutant, and *atg7-3/lip5-2/sid2* and *atg7-3/lip5-2/pad4* triple mutants.

Funding information

This work was supported by China National Major Research and Development Plan and Development Plan (grant no. 0111900) and Zhejiang Provincial Natural Science Foundation of China (grant no. LQ20C020002) at China Jiliang University and by the U.S. National Science Foundation (grant nos IOS1456300 and IOS1758767) at Purdue University.

Conflict of interest statement. None declared.

References

Allakhverdiev SI. Optimising photosynthesis for environmental fitness. Funct Plant Biol. 2020:**47**(11):iii–vii. https://doi.org/10.1071/FPv47n11_FO

An Q, Ehlers K, Kogel KH, van Bel AJ, Huckelhoven R. Multivesicular compartments proliferate in susceptible and resistant MLA12-barley leaves in response to infection by the biotrophic powdery mildew fungus. New Phytol. 2006:**172**(3):563–576. https://doi.org/10.1111/j.1469-8137.2006.01844.x

Anders S, Pyl PT, Huber W. HTSeq–a Python framework to work with high-throughput sequencing data. Bioinformatics. 2015:**31**(2):166–169. https://doi.org/10.1093/bioinformatics/btu638

Andres-Barrao C, Alzubaidy H, Jalal R, Mariappan KG, de Zelicourt A, Bokhari A, Artyukh O, Alwutayd K, Rawat A, Shekhawat K, et al. Coordinated bacterial and plant sulfur metabolism in Enterobacter sp. SA187-induced plant salt stress tolerance. Proc Natl Acad Sci U S A. 2021:**118**(46):e2107417118. https://doi.org/10.1073/pnas.2107417118

Armbruster U, Zuhlke J, Rengstl B, Kreller R, Makarenko E, Ruhle T, Schunemann D, Jahns P, Weisshaar B, Nickelsen J, et al. The Arabidopsis thylakoid protein PAM68 is required for efficient D1 biogenesis and photosystem II assembly. Plant Cell. 2010:**22**(10):3439–3460. https://doi.org/10.1105/tpc.110.077453

Aroca A, Yruela I, Gotor C, Bassham DC. Persulfidation of ATG18a regulates autophagy under ER stress in Arabidopsis. Proc Natl Acad Sci U S A. 2021:**118**(20):e2023604118. https://doi.org/10.1073/pnas.2023604118

Athanasiou K, Dyson BC, Webster RE, Johnson GN. Dynamic acclimation of photosynthesis increases plant fitness in changing environments. Plant Physiol. 2010:**152**(1):366–373. https://doi.org/10.1104/pp.109.149351

Bao Y, Bassham DC. ER-Phagy and its role in ER homeostasis in plants. Plants (Basel). 2020:**9**(12):1771. https://doi.org/10.3390/plants9121771

Berkey R, Zhang Y, Ma X, King H, Zhang Q, Wang W, Xiao S. Homologues of the RPW8 resistance protein are localized to the extrahaustorial membrane that is likely synthesized de novo. Plant Physiol. 2017:**173**(1):600–613. https://doi.org/10.1104/pp.16.01539

Bolger AM, Lohse M, Usadel B. Trimmomatic: a flexible trimmer for Illumina sequence data. Bioinformatics. 2014:**30**(15):2114–2120. https://doi.org/10.1093/bioinformatics/btu170

Chan KX, Phua SY, Crisp P, McQuinn R, Pogson BJ. Learning the languages of the chloroplast: retrograde signaling and beyond. Annu Rev Plant Biol. 2016:**67**(1):25–53. https://doi.org/10.1146/annurev-arplant-043015-111854

Chan KX, Phua SY, Van Breusegem F. Secondary sulfur metabolism in cellular signalling and oxidative stress responses. J Exp Bot. 2019:**70**-(16):4237–4250. https://doi.org/10.1093/jxb/erz119

Chaumont F, Tyerman SD. Aquaporins: highly regulated channels controlling plant water relations. Plant Physiol. 2014:**164**(4):1600–1618. https://doi.org/10.1104/pp.113.233791

Chen Z, Zhao PX, Miao ZQ, Qi GF, Wang Z, Yuan Y, Ahmad N, Cao MJ, Hell R, Wirtz M, et al. SULTR3s function in chloroplast sulfate uptake and affect ABA biosynthesis and the stress response. Plant Physiol. 2019:**180**(1):593–604. https://doi.org/10.1104/pp.18.01439

Cui H, Gobbato E, Kracher B, Qiu J, Bautor J, Parker JE. A core function of EDS1 with PAD4 is to protect the salicylic acid defense sector in Arabidopsis immunity. New Phytol. 2017:**213**(4):1802–1817. https://doi.org/10.1111/nph.14302

Cui Y, He Y, Cao W, Gao J, Jiang L. The multivesicular body and autophagosome pathways in plants. Front Plant Sci. 2018:**9**:1837. https://doi.org/10.3389/fpls.2018.01837

Cui Y, Shen J, Gao C, Zhuang X, Wang J, Jiang L. Biogenesis of plant prevacuolar multivesicular bodies. Mol Plant. 2016:**9**(6):774–786. https://doi.org/10.1016/j.molp.2016.01.011

Dagdas YF, Belhaj K, Maqbool A, Chaparro-Garcia A, Pandey P, Petre B, Tabassum N, Cruz-Mireles N, Hughes RK, Sklenar J, et al. An effector of the Irish potato famine pathogen antagonizes a host autophagy cargo receptor. Elife. 2016:**5**:e10856. https://doi.org/10.7554/eLife.10856

Dagdas YF, Pandey P, Tumtas Y, Sanguankiattichai N, Belhaj K, Duggan C, Leary AY, Segretin ME, Contreras MP, Savage Z, et al. Host autophagy machinery is diverted to the pathogen interface to mediate focal defense responses against the Irish potato famine pathogen. Elife. 2018:**7**:e37476. https://doi.org/10.7554/eLife.37476

Davidian JC, Kopriva S. Regulation of sulfate uptake and assimilation—the same or not the same? Mol Plant. 2010:**3**(2):314–325. https://doi.org/10.1093/mp/ssq001

Ding P, Rekhter D, Ding Y, Feussner K, Busta L, Haroth S, Xu S, Li X, Jetter R, Feussner I, et al. Characterization of a pipecolic acid biosynthesis pathway required for systemic acquired resistance. Plant Cell. 2016:**28**(10):2603–2615. https://doi.org/10.1105/tpc.16.00486

Droux M. Sulfur assimilation and the role of sulfur in plant metabolism: a survey. Photosynth Res. 2004:**79**(3):331–348. https://doi.org/10.1023/B:PRES.0000017196.95499.11

Duan J, Lee KP, Dogra V, Zhang S, Liu K, Caceres-Moreno C, Lv S, Xing W, Kato Y, Sakamoto W, et al. Impaired PSII proteostasis promotes retrograde signaling via salicylic acid. Plant Physiol. 2019:**180**(4):2182–2197. https://doi.org/10.1104/pp.19.00483

Fader CM, Colombo MI. Autophagy and multivesicular bodies: two closely related partners. Cell Death Differ. 2009:**16**(1):70–78. https://doi.org/10.1038/cdd.2008.168

Fink AL. Chaperone-mediated protein folding. Physiol Rev. 1999:**79**(2):425–449. https://doi.org/10.1152/physrev.1999.79.2.425

Foyer CH. Reactive oxygen species, oxidative signaling and the regulation of photosynthesis. Environ Exp Bot. 2018:**154**:134–142. https://doi.org/10.1016/j.envexpbot.2018.05.003

Fu Y, Li X, Fan B, Zhu C, Chen Z. Chloroplasts protein quality control and turnover: a multitude of mechanisms. Int J Mol Sci. 2022:**23**(14):7760. https://doi.org/10.3390/ijms23147760

Ganesan D, Cai Q. Understanding amphisomes. Biochem J. 2021:**478**-(10):1959–1976. https://doi.org/10.1042/BCJ20200917

Gao C, Luo M, Zhao Q, Yang R, Cui Y, Zeng Y, Xia J, Jiang L. A unique plant ESCRT component, FREE1, regulates multivesicular body protein sorting and plant growth. Curr Biol. 2014:**24**(21):2556–2563. https://doi.org/10.1016/j.cub.2014.09.014

Gao C, Zhuang X, Cui Y, Fu X, He Y, Zhao Q, Zeng Y, Shen J, Luo M, Jiang L. Dual roles of an Arabidopsis ESCRT component FREE1 in regulating vacuolar protein transport and autophagic degradation. Proc Natl Acad Sci U S A. 2015:**112**(6):1886–1891. https://doi.org/10.1073/pnas.1421271112

Ghosh S, Chan CK. Analysis of RNA-seq data using TopHat and Cufflinks. Methods Mol Biol. 2016:**1374**:339–361. https://doi.org/10.1007/978-1-4939-3167-5_18

Gotor C, Aroca A, Romero LC. Persulfidation is the mechanism underlying sulfide-signaling of autophagy. Autophagy 2021:**18**(3):1–3. https://doi.org/10.1080/15548627.2021.1936357

Guillaumot D, Guillon S, Morsomme P, Batoko H. ABA, porphyrins and plant TSPO-related protein. Plant Signal Behav. 2009:**4**(11):1087–1090. https://doi.org/10.4161/psb.4.11.9796

Haas TJ, Sliwinski MK, Martinez DE, Preuss M, Ebine K, Ueda T, Nielsen E, Odorizzi G, Otegui MS. The Arabidopsis AAA ATPase SKD1 is involved in multivesicular endosome function and interacts with its positive regulator LYST-INTERACTING PROTEIN5. Plant Cell. 2007:**19**(4):1295–1312. https://doi.org/10.1105/tpc.106.049346

Hachez C, Veljanovski V, Reinhardt H, Guillaumot D, Vanhee C, Chaumont F, Batoko H. The Arabidopsis abiotic stress-induced TSPO-related protein reduces cell-surface expression of the aquaporin PIP2; 7 through protein-protein interactions and autophagic degradation. Plant Cell. 2014:**26**(12):4974–4990. https://doi.org/10.1105/tpc.114.134080

Hanson PI, Cashikar A. Multivesicular body morphogenesis. Annu Rev Cell Dev Biol. 2012:**28**(1):337–362. https://doi.org/10.1146/annurev-cellbio-092910-154152

Have M, Luo J, Tellier F, Balliau T, Cueff G, Chardon F, Zivy M, Rajjou L, Cacas JL, Masclaux-Daubresse C. Proteomic and lipidomic analyses of the Arabidopsis atg5 autophagy mutant reveal major changes in endoplasmic reticulum and peroxisome metabolisms and in lipid composition. New Phytol. 2019:**223**(3):1461–1477. https://doi.org/10.1111/nph.15913

Hayat S, Hayat Q, Alyemeni MN, Wani AS, Pichtel J, Ahmad A. Role of proline under changing environments: a review. Plant Signal Behav. 2012:**7**(11):1456–1466. https://doi.org/10.4161/psb.21949

Hirai MY, Fujiwara T, Awazuhara M, Kimura T, Noji M, Saito K. Global expression profiling of sulfur-starved Arabidopsis by DNA macroarray reveals the role of O-acetyl-l-serine as a general regulator of gene expression in response to sulfur nutrition. Plant J. 2003:**33**(4):651–663. https://doi.org/10.1046/j.1365-313X.2003.01658.x

Howarth JR, Parmar S, Barraclough PB, Hawkesford MJ. A sulphur deficiency-induced gene, sdi1, involved in the utilization of stored sulphate pools under sulphur-limiting conditions has potential as a diagnostic indicator of sulphur nutritional status. Plant Biotechnol J. 2009:**7**(2):200–209. https://doi.org/10.1111/j.1467-7652.2008.00391.x

Huang J, Gu M, Lai Z, Fan B, Shi K, Zhou YH, Yu JQ, Chen Z. Functional analysis of the Arabidopsis PAL gene family in plant growth, development, and response to environmental stress. Plant Physiol. 2010:**153**(4):1526–1538. https://doi.org/10.1104/pp.110.157370

Huang XY, Chao DY, Koprivova A, Danku J, Wirtz M, Muller S, Sandoval FJ, Bauwe H, Roje S, Dilkes B, et al. Nuclear localised MORE SULPHUR ACCUMULATION1 epigenetically regulates sulphur homeostasis in *Arabidopsis thaliana*. PLoS Genet. 2016:**12**(9):e1006298. https://doi.org/10.1371/journal.pgen.1006298

Izumi M, Ishida H. The changes of leaf carbohydrate contents as a regulator of autophagic degradation of chloroplasts via Rubisco-containing bodies during leaf senescence. Plant Signal Behav. 2011:**6**(5):685–687. https://doi.org/10.4161/psb.6.5.14949

Izumi M, Nakamura S. Chloroplast protein turnover: the influence of extraplastidic processes, including autophagy. Int J Mol Sci. 2018:**19**(3):828. https://doi.org/10.3390/ijms19030828

Izumi M, Wada S, Makino A, Ishida H. The autophagic degradation of chloroplasts via rubisco-containing bodies is specifically linked to leaf carbon status but not nitrogen status in Arabidopsis. Plant Physiol. 2010:**154**(3):1196–1209. https://doi.org/10.1104/pp.110.158519

Jajic I, Sarna T, Strzalka K. Senescence, stress, and reactive oxygen species. Plants (Basel). 2015:**4**(3):393–411. https://doi.org/10.3390/plants4030393

James M, Poret M, Masclaux-Daubresse C, Marmagne A, Coquet L, Jouenne T, Chan P, Trouverie J, Etienne P. SAG12, a major cysteine protease involved in nitrogen allocation during senescence for seed production in *Arabidopsis thaliana*. Plant Cell Physiol. 2018:**59**(10):2052–2063. https://doi.org/10.1093/pcp/pcy125

Jiang SC, Engle NL, Banday ZZ, Cecchini NM, Jung HW, Tschaplinski TJ, Greenberg JT. ALD1 accumulation in Arabidopsis epidermal plastids confers local and non-autonomous disease resistance. J Exp Bot. 2021:**72**(7):2710–2726. https://doi.org/10.1093/jxb/eraa609

Kim D, Paggi JM, Park C, Bennett C, Salzberg SL. Graph-based genome alignment and genotyping with HISAT2 and HISAT-genotype. Nat Biotechnol. 2019:**37**(8):907–915. https://doi.org/10.1038/s41587-019-0201-4

Kim KC, Lai Z, Fan B, Chen Z. Arabidopsis WRKY38 and WRKY62 transcription factors interact with histone deacetylase 19 in basal defense. Plant Cell. 2008:**20**(9):2357–2371. https://doi.org/10.1105/tpc.107.055566

Kopriva S. 12-Oxo-phytodienoic acid interaction with cyclophilin CYP20-3 is a benchmark for understanding retrograde signaling in plants. Proc Natl Acad Sci U S A. 2013:**110**(23):9197–9198. https://doi.org/10.1073/pnas.1307482110

Kopriva S, Buchert T, Fritz G, Suter M, Weber M, Benda R, Schaller J, Feller U, Schurmann P, Schunemann V, et al. Plant adenosine 5′-phosphosulfate reductase is a novel iron-sulfur protein. J Biol Chem. 2001:**276**(46):42881–42886. https://doi.org/10.1074/jbc.M107424200

Kopriva S, Malagoli M, Takahashi H. Sulfur nutrition: impacts on plant development, metabolism, and stress responses. J Exp Bot. 2019:**70**(16):4069–4073. https://doi.org/10.1093/jxb/erz319

Lai Z, Wang F, Zheng Z, Fan B, Chen Z. A critical role of autophagy in plant resistance to necrotrophic fungal pathogens. Plant J. 2011:**66**(6):953–968. https://doi.org/10.1111/j.1365-313X.2011.04553.x

Lee BR, Huseby S, Koprivova A, Chetelat A, Wirtz M, Mugford ST, Navid E, Brearley C, Saha S, Mithen R, et al. Effects of fou8/fry1 mutation on sulfur metabolism: is decreased internal sulfate the trigger of sulfate starvation response? PLoS One. 2012:**7**(6):e39425. https://doi.org/10.1371/journal.pone.0039425

Lee BR, Koprivova A, Kopriva S. The key enzyme of sulfate assimilation, adenosine 5′-phosphosulfate reductase, is regulated by HY5 in Arabidopsis. Plant J. 2011:**67**(6):1042–1054. https://doi.org/10.1111/j.1365-313X.2011.04656.x

Leustek T. Sulfate metabolism. Arabidopsis Book. 2002:**1**:e0017. https://doi.org/10.1199/tab.0017

Leustek T, Saito K. Sulfate transport and assimilation in plants. Plant Physiol. 1999:**120**(3):637–644. https://doi.org/10.1104/pp.120.3.637

Li H, Li Y, Zhao Q, Li T, Wei J, Li B, Shen W, Yang C, Zeng Y, Rodriguez PL, et al. The plant ESCRT component FREE1 shuttles to the nucleus to attenuate abscisic acid signalling. Nat Plants. 2019:**5**(5):512–524. https://doi.org/10.1038/s41477-019-0400-5

Li X, Wang Z, Fu Y, Cheng X, Zhang Y, Fan B, Zhu C, Chen Z. Two ubiquitin-associated ER proteins interact with COPT copper transporters and modulate their accumulation. Plant Physiol. 2021:**187**(4):2469–2484. https://doi.org/10.1093/plphys/kiab381

Liang G, Yang F, Yu D. MicroRNA395 mediates regulation of sulfate accumulation and allocation in *Arabidopsis thaliana*. Plant J. 2010:**62**(6):1046–1057. https://doi.org/10.1111/j.1365-313X.2010.04216.x

Liu Y, Li J. Endoplasmic reticulum-mediated protein quality control in Arabidopsis. Front Plant Sci. 2014:**5**:162. https://doi.org/10.3389/fpls.2014.00162

Liu Y, Xiong Y, Bassham DC. Autophagy is required for tolerance of drought and salt stress in plants. Autophagy. 2009:**5**(7):954–963. https://doi.org/10.4161/auto.5.7.9290

Love MI, Huber W, Anders S. Moderated estimation of fold change and dispersion for RNA-seq data with DESeq2. Genome Biol. 2014:**15**(12):550. https://doi.org/10.1186/s13059-014-0550-8

Luo W, Brouwer C. Pathview: an R/Bioconductor package for pathway-based data integration and visualization. Bioinformatics. 2013:**29**(14): 1830–1831. https://doi.org/10.1093/bioinformatics/btt285

Lv F, Zhou J, Zeng L, Xing D. Beta-cyclocitral upregulates salicylic acid signalling to enhance excess light acclimation in Arabidopsis. J Exp Bot. 2015:**66**(15):4719–4732. https://doi.org/10.1093/jxb/erv231

Mao G, Meng X, Liu Y, Zheng Z, Chen Z, Zhang S. Phosphorylation of a WRKY transcription factor by two pathogen-responsive MAPKs drives phytoalexin biosynthesis in Arabidopsis. Plant Cell. 2011:**23**(4):1639–1653. https://doi.org/10.1105/tpc.111.084996

Maruyama-Nakashita A, Inoue E, Watanabe-Takahashi A, Yamaya T, Takahashi H. Transcriptome profiling of sulfur-responsive genes in Arabidopsis reveals global effects of sulfur nutrition on multiple metabolic pathways. Plant Physiol. 2003:**132**(2):597–605. https://doi.org/10.1104/pp.102.019802

Masclaux-Daubresse C, Clement G, Anne P, Routaboul JM, Guiboileau A, Soulay F, Shirasu K, Yoshimoto K. Stitching together the multiple dimensions of autophagy using metabolomics and transcriptomics reveals impacts on metabolism, development, and plant responses to the environment in Arabidopsis. Plant Cell. 2014:**26**(5): 1857–1877. https://doi.org/10.1105/tpc.114.124677

McLoughlin F, Augustine RC, Marshall RS, Li F, Kirkpatrick LD, Otegui MS, Vierstra RD. Maize multi-omics reveal roles for autophagic recycling in proteome remodelling and lipid turnover. Nat Plants. 2018:**4**(12):1056–1070. https://doi.org/10.1038/s41477-018-0299-2

McLoughlin F, Marshall RS, Ding X, Chatt EC, Kirkpatrick LD, Augustine RC, Li F, Otegui MS, Vierstra RD. Autophagy plays prominent roles in amino acid, nucleotide, and carbohydrate metabolism during fixed-carbon starvation in maize. Plant Cell. 2020:**32**(9): 2699–2724. https://doi.org/10.1105/tpc.20.00226

Michaeli S, Honig A, Levanony H, Peled-Zehavi H, Galili G. Arabidopsis ATG8-INTERACTING PROTEIN1 is involved in autophagy-dependent vesicular trafficking of plastid proteins to the vacuole. Plant Cell. 2014:**26**(10):4084–4101. https://doi.org/10.1105/tpc.114.129999

Mishina TE, Zeier J. The Arabidopsis flavin-dependent monooxygenase FMO1 is an essential component of biologically induced systemic acquired resistance. Plant Physiol. 2006:**141**(4):1666–1675. https://doi.org/10.1104/pp.106.081257

Mittler R, Zandalinas SI, Fichman Y, Van Breusegem F. Reactive oxygen species signalling in plant stress responses. Nat Rev Mol Cell Biol. 2022:**23**(10):663–679. https://doi.org/10.1038/s41580-022-00499-2

Muller M, Schmidt O, Angelova M, Faserl K, Weys S, Kremser L, Pfaffenwimmer T, Dalik T, Kraft C, Trajanoski Z, et al. The coordinated action of the MVB pathway and autophagy ensures cell survival during starvation. Elife. 2015:**4**:e07736. https://doi.org/10.7554/eLife.07736

Murchie EH, Lawson T. Chlorophyll fluorescence analysis: a guide to good practice and understanding some new applications. J Exp Bot. 2013:**64**(13):3983–3998. https://doi.org/10.1093/jxb/ert208

Nagel MK, Kalinowska K, Vogel K, Reynolds GD, Wu Z, Anzenberger F, Ichikawa M, Tsutsumi C, Sato MH, Kuster B, et al. Arabidopsis SH3P2 is an ubiquitin-binding protein that functions together with ESCRT-I and the deubiquitylating enzyme AMSH3. Proc Natl Acad Sci U S A. 2017:**114**(34):E7197–E7204. https://doi.org/10.1073/pnas.1710866114

Nikiforova V, Freitag J, Kempa S, Adamik M, Hesse H, Hoefgen R. Transcriptome analysis of sulfur depletion in *Arabidopsis thaliana*: interlacing of biosynthetic pathways provides response specificity. Plant J. 2003:**33**(4):633–650. https://doi.org/10.1046/j.1365-313X.2003.01657.x

Nolan TM, Brennan B, Yang M, Chen J, Zhang M, Li Z, Wang X, Bassham DC, Walley J, Yin Y. Selective autophagy of BES1 mediated by DSK2 balances plant growth and survival. Dev Cell. 2017:**41**(1): 33–46 e37. https://doi.org/10.1016/j.devcel.2017.03.013

Phua SY, Yan D, Chan KX, Estavillo GM, Nambara E, Pogson BJ. The Arabidopsis SAL1-PAP pathway: a case study for integrating chloroplast retrograde, light and hormonal signaling in modulating plant growth and development? Front Plant Sci. 2018:**9**:1171. https://doi.org/10.3389/fpls.2018.01171

Porra RJ, Thompson WA, Kriedemann PE. Determination of accurate extinction coefficients and simultaneous-equations for assaying chlorophyll-a and chlorophyll-B extracted with 4 different solvents—verification of the concentration of chlorophyll standards by atomic-absorption spectroscopy. Biochim Biophys Acta. 1989:**975**(3): 384–394. https://doi.org/10.1016/S0005-2728(89)80347-0

Putri GH, Anders S, Pyl PT, Pimanda JE, Zanini F. Analysing high-throughput sequencing data in Python with HTSeq 2.0. Bioinformatics. 2022:**38**(10):2943–2945. https://doi.org/10.1093/bioinformatics/btac166

Quintero FJ, Garciadeblas B, Rodriguez-Navarro A. The SAL1 gene of Arabidopsis, encoding an enzyme with 3′(2′),5′-bisphosphate nucleotidase and inositol polyphosphate 1-phosphatase activities, increases salt tolerance in yeast. Plant Cell. 1996:**8**(3):529–537. https://doi.org/10.1105/tpc.8.3.529

Ramel F, Birtic S, Ginies C, Soubigou-Taconnat L, Triantaphylides C, Havaux M. Carotenoid oxidation products are stress signals that mediate gene responses to singlet oxygen in plants. Proc Natl Acad Sci U S A. 2012:**109**(14):5535–5540. https://doi.org/10.1073/pnas.1115982109

Ramel F, Ksas B, Akkari E, Mialoundama AS, Monnet F, Krieger-Liszkay A, Ravanat JL, Mueller MJ, Bouvier F, Havaux M. Light-induced acclimation of the Arabidopsis chlorina1 mutant to singlet oxygen. Plant Cell. 2013:**25**(4):1445–1462. https://doi.org/10.1105/tpc.113.109827

Rietz S, Stamm A, Malonek S, Wagner S, Becker D, Medina-Escobar N, Corina Vlot A, Feys BJ, Niefind K, Parker JE. Different roles of Enhanced Disease Susceptibility1 (EDS1) bound to and dissociated from Phytoalexin Deficient4 (PAD4) in Arabidopsis immunity. New Phytol 2011:**191**(1):107–119. https://doi.org/10.1111/j.1469-8137.2011.03675.x

Rizhsky L, Liang H, Mittler R. The water-water cycle is essential for chloroplast protection in the absence of stress. J Biol Chem. 2003:**278**(40):38921–38925. https://doi.org/10.1074/jbc.M304987200

Rodriguez VM, Chetelat A, Majcherczyk P, Farmer EE. Chloroplastic phosphoadenosine phosphosulfate metabolism regulates basal levels of the prohormone jasmonic acid in Arabidopsis leaves. Plant Physiol. 2010:**152**(3):1335–1345. https://doi.org/10.1104/pp.109.150474

Romero LC, Aroca MA, Laureano-Marin AM, Moreno I, Garcia I, Gotor C. Cysteine and cysteine-related signaling pathways in *Arabidopsis thaliana*. Mol Plant. 2014:**7**(2):264–276. https://doi.org/10.1093/mp/sst168

Shilov IV, Seymour SL, Patel AA, Loboda A, Tang WH, Keating SP, Hunter CL, Nuwaysir LM, Schaeffer DA. The Paragon Algorithm, a next generation search engine that uses sequence temperature values and feature probabilities to identify peptides from tandem mass spectra. Mol Cell Proteomics. 2007:**6**(9):1638–1655. https://doi.org/10.1074/mcp.T600050-MCP200

Sirko A, Wawrzynska A, Rodriguez MC, Sektas P. The family of LSU-like proteins. Front Plant Sci. 2014:**5**:774. https://doi.org/10.3389/fpls.2014.00774

Spitzer C, Li F, Buono R, Roschzttardtz H, Chung T, Zhang M, Osteryoung KW, Vierstra RD, Otegui MS. The endosomal protein CHARGED MULTIVESICULAR BODY PROTEIN1 regulates the autophagic turnover of plastids in Arabidopsis. Plant Cell. 2015:**27**(2): 391–402. https://doi.org/10.1105/tpc.114.135939

Spitzer C, Reyes FC, Buono R, Sliwinski MK, Haas TJ, Otegui MS. The ESCRT-related CHMP1A and B proteins mediate multivesicular body sorting of auxin carriers in Arabidopsis and are required for plant development. Plant Cell. 2009:**21**(3):749–766. https://doi.org/10.1105/tpc.108.064865

Tabatabai MA, Bremner JM. Simple turbidimetric method of determining total sulfur in plant materials. Agron J. 1970:**62**(6):805. https://doi.org/10.2134/agronj1970.00021962006200060038x

Takahashi H, Kopriva S, Giordano M, Saito K, Hell R. Sulfur assimilation in photosynthetic organisms: molecular functions and regulations of transporters and assimilatory enzymes. Annu Rev Plant Biol. 2011:**62**(1):157–184. https://doi.org/10.1146/annurev-arplant-042110-103921

Thordal-Christensen H, Zhang ZG, Wei YD, Collinge DB. Subcellular localization of H2O2 in plants: H2O2 accumulation in papillae and hypersensitive response during the barley-powdery mildew interaction. Plant J. 1997:**11**(6):1187–1194. https://doi.org/10.1046/j.1365-313X.1997.11061187.x

Torrens-Spence MP, Bobokalonova A, Carballo V, Glinkerman CM, Pluskal T, Shen A, Weng JK. PBS3 And EPS1 complete salicylic acid biosynthesis from isochorismate in Arabidopsis. Mol Plant. 2019:**12**-(12):1577–1586. https://doi.org/10.1016/j.molp.2019.11.005

Triantaphylides C, Havaux M. Singlet oxygen in plants: production, detoxification and signaling. Trends Plant Sci. 2009:**14**(4):219–228. https://doi.org/10.1016/j.tplants.2009.01.008

Tsakraklides G, Martin M, Chalam R, Tarczynski MC, Schmidt A, Leustek T. Sulfate reduction is increased in transgenic *Arabidopsis thaliana* expressing 5′-adenylylsulfate reductase from *Pseudomonas aeruginosa*. Plant J. 2002:**32**(6):879–889. https://doi.org/10.1046/j.1365-313X.2002.01477.x

Ueda M, Tsutsumi N, Fujimoto M. Salt stress induces internalization of plasma membrane aquaporin into the vacuole in *Arabidopsis thaliana*. Biochem Biophys Res Commun. 2016:**474**(4):742–746. https://doi.org/10.1016/j.bbrc.2016.05.028

Van Breusegem F, Dat JF. Reactive oxygen species in plant cell death. Plant Physiol. 2006:**141**(2):384–390. https://doi.org/10.1104/pp.106.078295

Volkel S, Grieshaber MK. Mechanisms of sulfide tolerance in the peanut worm, *Sipunculus nudus* (Sipunculidae) and in the lugworm, *Arenicola marina* (Polychaeta). J Comp Physiol B Biochem Syst Environ Physiol. 1992:**162**:469–477. https://doi.org/10.1007/BF00258971

Wang F, Shang Y, Fan B, Yu JQ, Chen Z. Arabidopsis LIP5, a positive regulator of multivesicular body biogenesis, is a critical target of pathogen-responsive MAPK cascade in plant basal defense. PLoS Pathog. 2014:**10**(7):e1004243. https://doi.org/10.1371/journal.ppat.1004243

Wang F, Yang Y, Wang Z, Zhou J, Fan B, Chen Z. A critical role of lyst-interacting Protein5, a positive regulator of multivesicular body biogenesis, in plant responses to heat and salt stresses. Plant Physiol. 2015:**169**(1):497–511. https://doi.org/10.1104/pp.15.00518

Wang M, Li X, Luo S, Fan B, Zhu C, Chen Z. Coordination and crosstalk between autophagosome and multivesicular body pathways in plant stress responses. Cells. 2020:**9**(1):119. https://doi.org/10.3390/cells9010119

Wang Y, Liu Y. Autophagic degradation of leaf starch in plants. Autophagy. 2013:**9**(8):1247–1248. https://doi.org/10.4161/auto.25176

Wang Z, Li X, Liu N, Peng Q, Wang Y, Fan B, Zhu C, Chen Z. A family of NAI2-interacting proteins in the biogenesis of the ER body and related structures. Plant Physiol. 2019:**180**(1):212–227. https://doi.org/10.1104/pp.18.01500

Yin ZY, Pascual C, Klionsky DJ. Autophagy: machinery and regulation. Microb Cell. 2016:**3**(12):457–465. https://doi.org/10.15698/mic2016.12.546

Yoshimoto K, Jikumaru Y, Kamiya Y, Kusano M, Consonni C, Panstruga R, Ohsumi Y, Shirasu K. Autophagy negatively regulates cell death by controlling NPR1-dependent salicylic acid signaling during senescence and the innate immune response in Arabidopsis. Plant Cell. 2009:**21**(9):2914–2927. https://doi.org/10.1105/tpc.109.068635

Yu F, Lou L, Tian M, Li Q, Ding Y, Cao X, Wu Y, Belda-Palazon B, Rodriguez PL, Yang S, et al. ESCRT-I component VPS23A affects ABA signaling by recognizing ABA receptors for endosomal degradation. Mol Plant. 2016:**9**(12):1570–1582. https://doi.org/10.1016/j.molp.2016.11.002

Yu G, Wang LG, Han Y, He QY. Clusterprofiler: an R package for comparing biological themes among gene clusters. OMICS. 2012:**16**(5):284–287. https://doi.org/10.1089/omi.2011.0118

Zeng Y, Li B, Zhang W, Jiang L. ER-Phagy and ER stress response (ERSR) in plants. Front Plant Sci. 2019:**10**:1192. https://doi.org/10.3389/fpls.2019.01192

Zhang H, Zhou JF, Kan Y, Shan JX, Ye WW, Dong NQ, Guo T, Xiang YH, Yang YB, Li YC, et al. A genetic module at one locus in rice protects chloroplasts to enhance thermotolerance. Science. 2022:**376**-(6599):1293–1300. https://doi.org/10.1126/science.abo5721

Zhang X, Ding X, Marshall RS, Paez-Valencia J, Lacey P, Vierstra RD, Otegui MS. Reticulon proteins modulate autophagy of the endoplasmic reticulum in maize endosperm. Elife. 2020:**9**:e51918. https://doi.org/10.7554/eLife.51918

Zhang Y, Fernie AR. On the role of the tricarboxylic acid cycle in plant productivity. J Integr Plant Biol. 2018:**60**(12):1199–1216. https://doi.org/10.1111/jipb.12690

Zhao C, Wang Y, Chan KX, Marchant DB, Franks PJ, Randall D, Tee EE, Chen G, Ramesh S, Phua SY, et al. Evolution of chloroplast retrograde signaling facilitates green plant adaptation to land. Proc Natl Acad Sci U S A. 2019:**116**(11):5015–5020. https://doi.org/10.1073/pnas.1812092116

Zhong Q, Hu H, Fan B, Zhu C, Chen Z. Biosynthesis and roles of salicylic acid in balancing stress response and growth in plants. Int J Mol Sci. 2021:**22**(21):11672. https://doi.org/10.3390/ijms222111672

Zhou J, Liu D, Wang P, Ma X, Lin W, Chen S, Mishev K, Lu D, Kumar R, Vanhoutte I, et al. Regulation of Arabidopsis brassinosteroid receptor BRI1 endocytosis and degradation by plant U-box PUB12/PUB13-mediated ubiquitination. Proc Natl Acad Sci U S A. 2018:**115**(8):E1906–E1915. https://doi.org/10.1073/pnas.1712251115

Zhou J, Wang J, Cheng Y, Chi YJ, Fan B, Yu JQ, Chen Z. NBR1-mediated selective autophagy targets insoluble ubiquitinated protein aggregates in plant stress responses. PLoS Genet. 2013:**9**(1):e1003196. https://doi.org/10.1371/journal.pgen.1003196

Zhou J, Zhang Y, Qi J, Chi Y, Fan B, Yu JQ, Chen Z. E3 ubiquitin ligase CHIP and NBR1-mediated selective autophagy protect additively against proteotoxicity in plant stress responses. PLoS Genet. 2014:**10**(1):e1004116. https://doi.org/10.1371/journal.pgen.1004116

Zhuang X, Wang H, Lam SK, Gao C, Wang X, Cai Y, Jiang L. A BAR-domain protein SH3P2, which binds to phosphatidylinositol 3-phosphate and ATG8, regulates autophagosome formation in Arabidopsis. Plant Cell. 2013:**25**(11):4596–4615. doi:10.1105/tpc.113.118307